Environmental Science and Pollution Research (2018) 25:24726–24745
https://doi.org/10.1007/s11356-018-2502-4

RESEARCH ARTICLE

Aerosol columnar characteristics and their heterogeneous nature over Varanasi, in the central Ganges valley

Shani Tiwari[1,2] · Dimitris Kaskaoutis[3] · Vijay Kumar Soni[4] · Shiv Dev Attri[4] · Abhay Kumar Singh[1,5]

Received: 23 November 2017 / Accepted: 4 June 2018 / Published online: 20 June 2018

Abstract

The Indo–Gangetic Basin (IGB) experiences one of the highest aerosol loading over the globe with pronounced inter-/intra-seasonal variability. Four-year (January 2011–December 2014) continuous MICROTOPS-II sun-photometer measurements at Varanasi, central Ganges valley, provide an opportunity to investigate the aerosol physical and optical properties and their variability. A large variation in aerosol optical depth (AOD: from 0.23 to 1.89, mean of 0.82 ± 0.31) and Ångström exponent (AE: from 0.19 to 1.44, mean of 0.96 ± 0.27) is observed, indicating a highly turbid atmospheric environment with significant heterogeneity in aerosol sources, types and optical properties. The highest seasonal means of both AOD and AE are observed in the post-monsoon (October–November) season (0.95 ± 0.31 for AOD and 1.16 ± 0.14 for AE) followed by winter (December, January, February; 0.97 ± 0.34 for AOD and 1.09 ± 0.20 for AE) and are mainly attributed to the accumulation of aerosols from urban and biomass/crop residue burning emissions within a shallow boundary layer. In contrast, during the pre-monsoon and monsoon seasons, the aerosols are mostly coming from natural origin (desert and mineral dust) mixed with pollution in several cases. The spectral dependence of AE, the aerosol "curvature" effect and other graphical techniques are used for the identification of the aerosol types and their mixing processes in the atmosphere. Furthermore, the aerosol source–apportionment assessment using the weighted potential source contribution function (WPSCF) analysis reveals the different aerosol types, emission sources and transport pathways.

Keywords Aerosol properties · Aerosol types · Seasonality · Source apportionment · Indo–Gangetic Basin

Introduction

Atmospheric aerosols, one of the key constituents of the Earth's atmosphere, play a vital role in global and regional climate change through their direct (scattering and absorption of solar and long wave radiation), indirect (change of cloud optical properties and lifetime), and semi-direct effects (evaporation of cloud droplet due to light absorption and heating) (Altaratz et al. 2014; Grandey et al. 2013; Rosenfeld et al. 2008; Schwartz et al. 1995; Seinfeld et al. 2016; Twomey 1991). They also have sufficient potential to affect the general atmospheric circulation patterns and bio-geochemical cycling (Lau et al. 2006; Mahowald 2011). However, the climate impacts of atmospheric aerosols associated with large spatial distribution and heterogeneity are closely related to their large uncertainties due to different emission sources, atmospheric mixing, and chemical transformation processes, as well as impacts on the regional meteorological conditions (IPCC 2013; Myhre et al. 2009). During the last few years, the uncertainties in quantifying the aerosol radiative impacts have

Responsible editor: Gerhard Lammel

Electronic supplementary material The online version of this article (https://doi.org/10.1007/s11356-018-2502-4) contains supplementary material, which is available to authorized users.

✉ Abhay Kumar Singh
abhay_s@rediffmail.com

[1] Atmospheric Research Laboratory, Department of Physics, Banaras Hindu University, Varanasi 221005, India

[2] Present Address: Graduate School of Environmental Studies, Nagoya University, Nagoya, Japan

[3] Atmospheric Research Team, Institute for Environmental Research and Sustainable Development, National Observatory of Athens, 11810 Athens, Greece

[4] India Meteorological Department, New Delhi 110001, India

[5] DST-Mahamana Centre of Excellence in Climate Change Research, B.H.U, Varanasi 221005, India

been decreased (IPCC 2013), but not up to the desired level. Therefore, assessing the quantification of the aerosol impact on climate is one of the most challenging issues in atmospheric science due to the different complex non-linear interactions between aerosol, solar radiation, clouds, and precipitation (Huang et al. 2006; IPCC 2013; Tiwari et al. 2016a). For better understanding of the aerosol effects, especially over high aerosol-laden atmospheres such as north India, it is essential to examine their physical, chemical, and optical properties at very high spatio-temporal resolutions and for long periods (Tiwari et al. 2009; Kaskaoutis et al. 2013; Lodhi et al. 2013; Mishra and Shibata 2012; Moorthy et al. 2013; Tiwari et al. 2016a).

The aerosol properties at any location are highly dependent on the emission sources and the regional meteorological conditions that are associated with aerosol mixing (external and internal) (Srivastava and Ramachandran 2013). South and East Asia (mainly India and China) experience heavy aerosol loading, which is continuously increasing during the past few decades due to large urbanization and continuous increase in population density and related energy demands (Dey and Di Girolamo 2010; Kang et al. 2016; Kaskaoutis et al. 2012a; Lawrence and Lelieveld 2010; Lin and Li 2016; Moorthy et al. 2013). India, and more particularly the Indo–Gangetic Basin (IGB), experience very high aerosol loading with a strong intra-seasonal to inter-annual variability (Kaskaoutis et al. 2012b; Lodhi et al. 2013; Prasad et al. 2007; Sharma et al. 2014; Singh et al. 2004; Tiwari et al. 2016a). Due to unique topography and seasonally changed meteorological conditions, IGB is a very interesting source region for aerosol studies and related climate implications (Meehl et al. 2008; (Dumka et al. 2014; Gautam et al. 2010, 2011, 2013; Giles et al. 2011; Kaskaoutis et al. 2014a; Singh et al. 2016; Srivastava et al. 2011; Tiwari et al. 2015a)). During the pre-monsoon (March–mid-June) season, IGB is strongly affected by frequent and intense dust storms through long-range transport from Arabia, southwest Asia, and the Thar Desert, which enhance the coarse-mode aerosol concentrations (Gautam et al. 2009; Pandithurai et al. 2008; Singh et al. 2016; Tiwari et al. 2015b). During the monsoon (mid/end of June–September) season, relatively lower aerosol concentrations are reported in most of the studies due to rainy washout and weakening in local dust re-suspension due to wet soil (Dey and Di Girolamo 2010; Lodhi et al. 2013; Tiwari and Singh 2013). However, a large inter-annual variability in monsoonal aerosol loading was observed over the IGB due to yearly changes in the onset, duration, and intensity of the monsoon and the presence of exceptional dry years (e.g. 2002 and 2004) (Kaskaoutis et al. 2012a). During the post-monsoon (October–November) season, crop residue burning is a common practice over the north-western IGB (Haryana and Punjab states), which leads to very high aerosol concentrations, mainly in the fine mode (Mishra and Shibata 2012; Sharma et al. 2010; Tiwari et al. 2016a). In association with favorable meteorological conditions, these particles form a dense smoke plume that covers the whole IGB, central-south India, and the coastal regions (Badarinath et al. 2009; Kaskaoutis et al. 2014b; Kharol et al. 2012). During winter (December–February), majority of the days in IGB are covered by fog and haze due to weak convection, high relative humidity, calm winds, and a shallow atmospheric boundary layer (Das et al. 2008; Gautam et al. 2007; Mishra and Shibata 2012). Different aerosol modification processes along with formation of secondary aerosol occur throughout the year, leading to a well-mixed boundary layer or lower troposphere with a diverse mixture of aerosol types or particle sizes (Dey et al. 2008; Srivastava and Ramachandran 2013). The mixing between mineral or desert dust with carbonaceous aerosols from different emission sources results in the formation of a thick aerosol layer, popularly referred to as atmospheric brown clouds (Ramanathan et al., 2005; Bonasoni et al. 2010). Therefore, to investigate the aerosol behavior and discriminate various aerosol types over IGB is a quite challenging task because of the different dynamic meteorological processes and emission sources that govern their concentrations and chemical composition. In this respect, a network of ground-based aerosol measurements has been established by the Indian Space Research Organization (ISRO) across the country (> 36 stations) under the Aerosol Radiative Forcing over India (ARFI) program in order to characterize different types of aerosols and their seasonality and trends (Babu et al. 2013; Moorthy et al. 1999, 2013). Therefore, sun photometric observations of aerosol columnar properties have been widely conducted over the Indian subcontinent (e.g., (Dani et al. 2012; Kaskaoutis et al. 2009, 2013; Kedia and Ramchandran 2011; Moorthy et al. 2013; Tiwari and Singh 2013; Tiwari et al. 2015b, 2016a).

The present study aims to examine the aerosol optical properties and their seasonality during a 4-year period (January 2011–December 2014) over Varanasi, India, using MICROTOPS -II sun-photometer measurements. Furthermore, the aerosol modification processes and classification of different aerosol types is attempted for the first time over this site. The HYbrid Single-Particle Lagrangian Integrated Trajectories (HYSPLIT) model is used along with the weighted potential source contribution function (WPSCF) analysis in order to examine the aerosol source apportionment and to quantify the contribution of different aerosol emission sources and transportation mechanisms. The current results are extensively compared with previous findings from several aerosol studies over the IGB and the Indian subcontinent, thus contributing to filling the aerosol database of the ARFI project.

Site description and meteorological condition

Varanasi (25.2° N, 82.9° E, 83 m above msl) is a city lying on the bank of Ganges river, in the central IGB. Varanasi has high

population density; 2399 residents per square kilometer (Census India; 2011) and is heavily polluted and aerosol laden throughout the year (Prasad et al. 2006; Tiwari and Singh 2013; Tiwari et al. 2015a). Large-scale uncontrolled urbanization, industrial development, and bio-fuel combustions are among the major causes for air, water, and land pollution over IGB and surrounding countryside (Prasad et al. 2006; Vaishya et al. 2017). Higher aerosol loading is observed over the entire IGB, including Varanasi, during the pre-monsoon season (Prasad et al. 2007; Singh et al. 2004; Tiwari and Singh 2013) due to the contribution of transported dust over an urban aerosol layer leading to relatively higher radiative forcing at the surface (Kaskaoutis et al. 2013; Sarkar et al. 2006; Srivastava et al. 2011). On certain occasions, Varanasi can be also influenced by marine aerosols transported from the Bay of Bengal during the rainy monsoon season (Tiwari and Singh 2013).

Figure 1 shows the daily and monthly mean variation of the meteorological parameters, i.e., (a) relative humidity, (b) temperature, (c) wind direction, and (d) wind speed, over Varanasi for January 2011–December 2014 obtained from India Meteorological Department (IMD). In spite of being a sub-tropical site, there is a remarkable seasonality in all the examined meteorological variables, which, however, exhibit similar patterns and values in each year. In this respect, the minimum relative humidity is always observed in pre-monsoon (April 38 ± 4%) and continuously increases during monsoon, reaching a maximum in the month of August (82 ± 3%). The minimum temperature occurs in January (14 ± 1 °C) and increases continuously until May (34 ± 1 °C) and then slightly decreases during monsoon and post-monsoon reaching a minimum in winter. The wind speed is rather low (< 3 ms^{-1} on monthly mean basis), having its maximum values during the late pre-monsoon and monsoon seasons (maximum in June of 2.56 ± 0.42 ms^{-1}). At this time, the wind blows from south–southeastern directions carrying humid air masses from the Bay of Bengal. During the study period, the monsoon season seems to start earlier in 2011 (mid of May) compared to 2012 (mid-June), (Pai and Bhan 2012) as observed from the earliest change in the wind direction (from west to southeast) and the earliest increase in the wind speed in 2011. Therefore, the onset and duration of the monsoon, as well as its intensity in view of rainy days and rainfall amounts, play an important role in the meteorological conditions over the IGB and influence the aerosol loading and properties (Gautam et al. 2009; Kaskaoutis et al. 2012a). Calm to weak winds from northwestern directions during the post-monsoon and winter seasons (minimum of 1.05 ± 0.24 ms^{-1}in November), cause unfavorable conditions for aerosol dispersion, thus helping the temperature inversions and accumulation of aerosol and pollutants near the ground (Komppula et al. 2012; Misra et al. 2012).

Instrumentation and data analysis

The ground-based spectral aerosol optical depth (AOD) measurements were carried out continuously from January 2011 to December 2014 under a clear sky using a handheld portable multiband sun-photometer MICROTOPS-II (Solar Light Company, USA). The MICROTOPS-II contains five different interference filters at 380-, 440-, 500-, 675-, and 870-nm wavelengths and provides columnar information about aerosols. The sun-photometer works on the principle of extinction of solar radiation intensity at a certain wavelength and has a Full Width at Half Maximum (FWHM) bandwidth of 2.4 ± 0.4 nm at a 380-nm channel and 10 ± 0.15 at the other channels. The field of view (FOV) is 2.5° with a typical sun targeting accuracy better than 0.1°. The error in the AOD retrievals in the UV is in the order of ± 0.03, which drops at ± 0.02 in the visible, since the long-term stability of the filter is better than 0.1 nm per year. More details about the MICROTOPS-II characteristics, its calibration, performance, and accuracy of the retrievals are given elsewhere (Morys et al. 2001; Singh et al. 2010).

The factory-calibrated instrument is deployed and operated at the Department of Physics, Banaras Hindu University, Varanasi, since 2011 and is calibrated periodically once per 2 years from Solar Light Company, USA. Sun-photometer measurements were deployed at every half hour from 9:00h to 16:00h LST on clear-sky conditions. In order to minimize aiming and cloud contamination errors, triplet Sun-photometer measurements were taken during each observation; higher values obtained via this procedure are discarded, because smaller values correspond to the most accurate Sun pointing (Porter et al. 2001). To avoid any possible cloud contamination, measurements were only done on clear days, with few or no clouds covering the sky, particularly at angles close to the Sun. Further, we applied the second-order polynomial fitting to the scanned MICROTPS data and select only those data which have maximum correlation ($r > 0.97$) and minimum error in second-order coefficient (Sharma et al. 2014). Out of the 4-year period, 844 days allowed sun photometric observations with a total number of 3455 scans.

The spectral AOD and the Angstrom Exponent (AE) are the two main parameters for examining the columnar aerosol loading and properties. The AE provides useful information about the aerosol size distribution and can be easily determined via the Angstrom power law (Angstrom 1964):

$$\tau_\lambda = \beta\lambda^{-\alpha} \quad (1)$$

where τ_λ is the AOD at wavelength λ expressed in micrometer (μm), α is the AE, and β the turbidity coefficient, which equals to AOD at $\lambda = 1$ μm. The AE is a relatively good indicator of the aerosol particle size and fraction of fine- to coarse-mode aerosols (Kaskaoutis et al. 2009; Schuster et al.

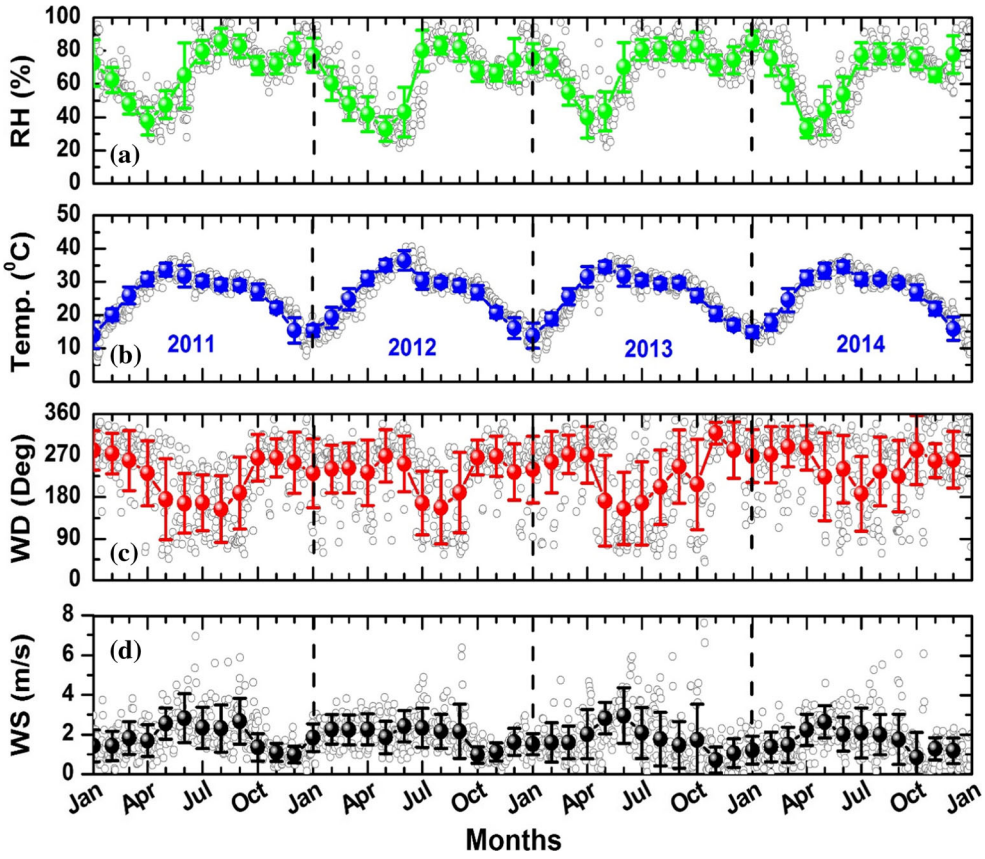

Fig. 1 Variation in meteorological parameters, i.e. **a** relative humidity, **b** temperature, **c** wind direction, and **d** wind speed, during the study period over Varanasi. The empty and filled spheres represent the daily and monthly variation while vertical lines represent standard deviation from their monthly mean

2006; Tiwari et al. 2015a, 2016). The Eq. (1) is valid and well fitted only for a limited wavelength range, where the columnar aerosol size distribution follows the Junge power law. However, for a wide wavelength range, a significant deviation in Eq. (1) is found, particularly for multimodal size distributions, suggesting heterogeneity in aerosol types due to different sources. The multimodal size distribution leads to the departure from linearity in the ln(AOD) vs ln(λ) curve, resulting in different AE values for different wavelength ranges (Beegum et al. 2009; Eck et al. 1999; Kaskaoutis et al. 2007, 2009; Reid et al. 1999). Under such conditions, a second-order polynomial fit can be applied to AOD spectra, which can be used to quantify the curvature in the spectral distribution of AOD (Eck et al. 1999; Kaskaoutis and Kambezidis 2006). Therefore, a second-order polynomial fit was applied to the $\ln\tau_\lambda$ vs ln λ data as:

$$\ln\tau_\lambda = A_2[\ln(\lambda)]^2 + A_1\ln(\lambda) + A_0 \quad (2)$$

where the coefficient A_2 represents the curvature. Negative values of A_2 indicate aerosol size distributions dominated by fine modes and positive values are indicative for size distributions clearly dominated by coarse-mode particles (Eck et al. 1999; Kaskaoutis et al. 2007; Kaskaoutis et al. 2009). Although Eq. (2) is more precise than Eq. (1) for a wide spectral range, yet large errors may occur especially for low turbidity conditions (Kaskaoutis et al. 2007). Therefore, in order to minimize these errors, only those data that attain a second-order polynomial fit with r values ≥ 0.97 and associated with minimum errors in the curvature (A_2) were considered in the current analysis. Figure 2a shows the correlation between typical errors in the coefficients A_1 and A_2 computed in the wavelength range 380–870 nm and AOD_{500} for all the examined scans during the study period. The results show that the larger errors in both A_1 and A_2 are associated with lower AODs, while they decrease significantly as the AOD increases. Similar results were also reported at other places using sun-photometer observations (Kaskaoutis et al. 2010; Sharma et al. 2014; Soni et al. 2011). The errors are minimized during the winter season and are largest in monsoon and post-monsoon, indicating a larger departure from the Ångström power law in these seasons and larger uncertainties in the spectral AOD retrievals. Figure 2b shows the scatter plot between the difference of the second-order polynomial coefficients (i.e., A_2–A_1) and AE (380–870 nm) for each scan on a seasonal basis. According to Schuster et al. (2006) and the verifications later on (e.g., (Kaskaoutis et al. 2007, 2010, 2011; Patel et al. 2017; Sharma et al. 2014)), A_2–A_1 equals to the AE for the same wavelength band, while an excellent linear regression between them suggests a high accuracy in the spectral AOD retrievals. The current results show very good performance between A_2–A_1 and AE, ($r > 0.94$) during all

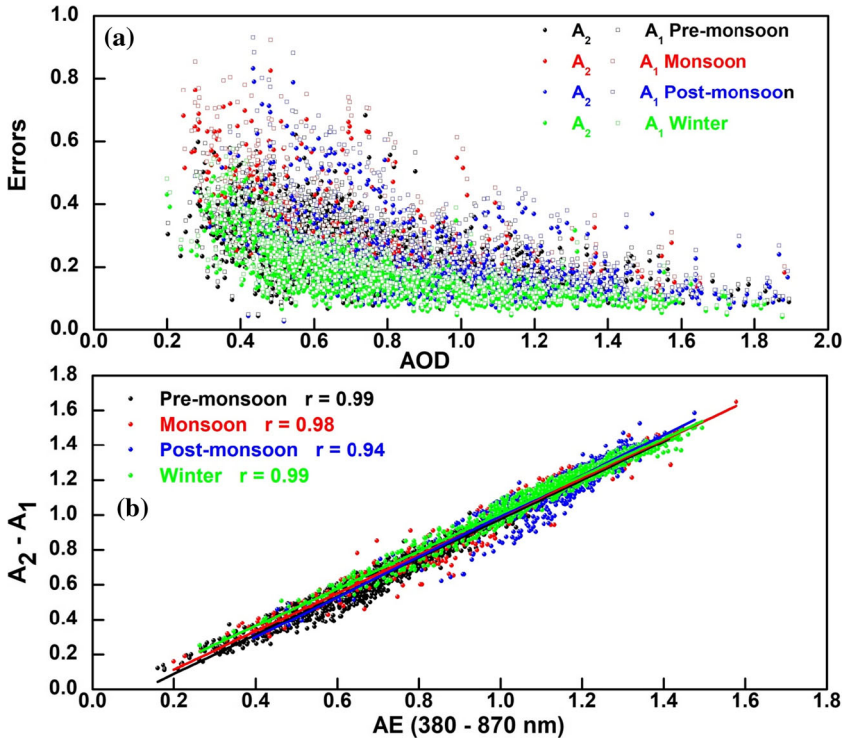

Fig. 2 Correlation between errors in the second-order polynomial fit and AOD (**a**) and between the coefficients A_2–$A_1$and AE (380–870 nm) (**b**) for the whole set of measurements in each season

seasons, suggesting minimum errors in the parameters computed from the spectral MICROTOPS-II AOD measurements.

Results and discussion

Variation in AOD and AE

Figure 3 shows the daily mean variation of AOD_{500} as a function of the $AE_{380–870}$ (in colored scale) over Varanasi during 2011–2014. The results reveal a wide range in both AOD_{500} (0.23–1.89) and AE (0.19–1.44) with mean values of 0.82 ± 0.31 and 0.96 ± 0.26, respectively. Such a large variation in aerosol loading suggests very differing atmospheric conditions in the view of aerosol emission sources and types and seasonally changed meteorological conditions over central IGB (Kaskaoutis et al. 2013; Tiwari et al. 2016a). Nearly 44% of the days exhibit AOD values above the mean, while the AE values are greater than the mean on 55% of the days. Earlier studies reported a little higher fraction for high AOD (> 0.6) over New Delhi (76%) (Tiwari et al. 2016a) and Greater Noida (70%) (Sharma et al. 2014) indicating more turbid conditions around the national capital region. Very high AODs, i.e., AOD > mean AOD + 1 standard deviation (σ) are shown in nearly 18% of the days, while on these days the fraction for AE >1.0 was 67%. This indicates that the very turbid conditions over Varanasi are mostly attributed to enhancement of the fine –mode anthropogenic or biomass burning aerosols during post-monsoon and winter (see Suppl. Fig.1), which contribute to the already high-background aerosol levels over central IGB. Suppl. Fig.1 clearly shows a larger gradient in AOD towards shorter wavelengths during the high-aerosol loading days (HAOD AOD > mean + 1σ) against the lower-aerosol loading days (LAOD, AOD < mean − 1σ) and annual mean (all days considered). Lower values of AE, associated with a similar range of AOD_{500}, are shown during April–June, which reflect the influence of the transported dust plumes carrying higher concentrations of coarser particles from the Thar Desert and Arabia. Earlier studies also reported the dominance of coarse particles over IGB during pre-monsoon due to dust storms from the west (Kaskaoutis et al. 2013; Lodhi et al. 2013; Singh et al. 2004, 2016; Soni et al. 2011; Tiwari and Singh 2013; Tiwari et al. 2016a). More than 50% days of the study period, AE values are higher than one which is more prominent in post-monsoon (nearly 91% days) and winter (nearly 75% days) season suggesting relatively higher concentration of fine mode particles throughout the year. On the other hand, in pre-monsoon season, nearly 60% days, AE values are less than 0.8 suggesting a mixture of fine- and coarse-mode particles. In addition, minimum AE values along with high AODs (mostly > 0.7) are observed during the end of June and in the monsoon period (July–September), indicating dominance of coarse-mode particles and possibility of hygroscopic growth of the fine-mode aerosols under a humid environment. In this respect, Tiwari and Singh (2013) found an association between higher concentrations of coarse aerosols and columnar water vapor over Varanasi during the monsoon season. Singh et al. (2004) and Tiwari et al. (2016a)

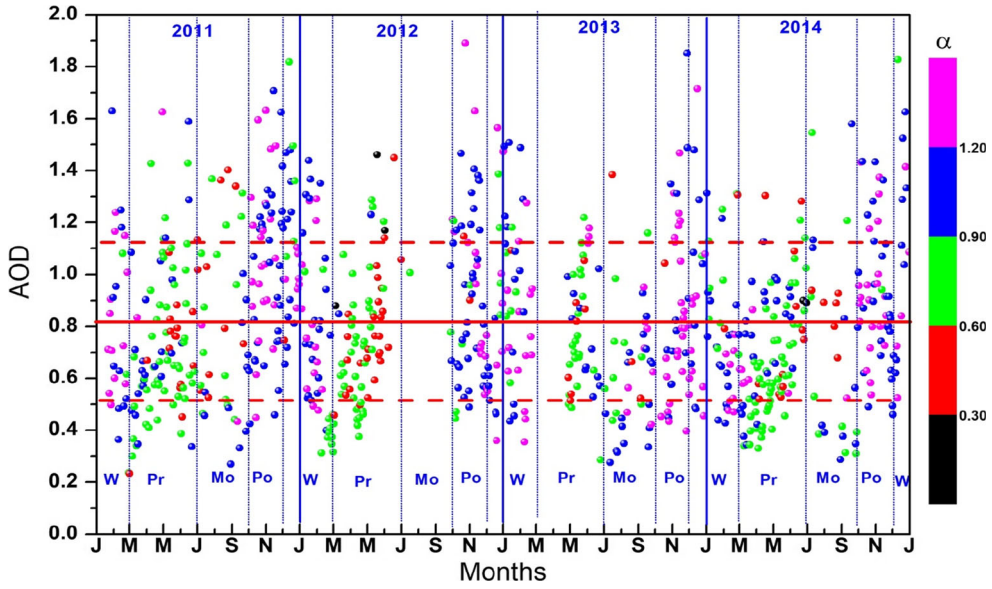

Fig. 3 Variation of daily-averaged AOD_{500} over Varanasi during January 2011–December 2014. The colored scale represents the daily mean values of the $AE_{380–870}$. The solid red line represents the annual mean, while the dash red lines represent the $\pm 1\sigma$ from the mean during the study period

also suggested the possibility of hygroscopic growth of the fine anthropogenic aerosols in Kanpur and New Delhi, respectively during the humid monsoon season, while maximum aerosol loading during July is reported at Greater Noida, Delhi outskirts (Sharma et al. 2014).

The AOD_{500} and $AE_{380–870nm}$ values from the current work are compared on a seasonal basis with those over several other sites in India, with emphasis over the IGB and the results are summarized in Table 1. Maximum seasonal AOD_{500} in the post-monsoon season was found over Varanasi highlighting the strong influence of the agricultural crop-residue burning in Punjab and the accumulation of a smoke plume over the whole IGB for several weeks (Kaskaoutis et al. 2014b). Similar results are also reported at other places over IGB, like Delhi (Lodhi et al. 2013; Tiwari et al. 2016a), Greater Noida (Sharma et al. 2014), and Kanpur (Kaskaoutis et al. 2013). The seasonal AOD values at Varanasi are quite comparable to those found in Greater Noida (Sharma et al. 2014) and Kharagpur (Pani and Verma 2014) and slightly lower than those reported for New Delhi (Tiwari et al. 2016a). The comparison with previous studies indicates that Varanasi has higher AODs than several other locations in IGB and the rest of the Indian subcontinent (Bhaskar et al. 2015; Dani et al. 2012; Guleria et al. 2012; Kannemadugu et al. 2015; Kaskaoutis et al. 2012a; Ram et al. 2010; Reddy et al. 2016; Srivastava et al. 2011) rendering it as one of the most polluted and aerosol-laden urban environments in India. Previous studies also reported higher values of AE during the post-monsoon and winter seasons over the IGB and other Indian regions (Kaskaoutis et al. 2014b; Kumar et al. 2015; Sharma et al. 2010; Tiwari and Singh 2013; Tiwari et al. 2016a). It should be noted here that some differences in the magnitudes of the AOD and AE values summarized in Table 1 could be also attributed to the different geographical locations, meteorological conditions, time of observations, instrumentation techniques, and wavelength regions used for the AE retrievals.

Figure 4 shows the monthly mean variation of AOD_{500} and $AE_{380–870}$ (a) and the seasonal mean spectral variation of AOD (b) over Varanasi during 2011–2014. The associated vertical bars represent $\pm 1\sigma$ from the respective mean values. Figure 4a exhibits a distinct annual pattern for AOD with two maxima during late pre-monsoon (May–June) and late post-monsoon/winter (November–January). This is very similar to those found over Kanpur (Kaskaoutis et al. 2013; Singh et al. 2004), Delhi (Lodhi et al. 2013), and Greater Noida (Sharma et al. 2014). The primary maximum in late post-monsoon/winter is associated with crop residue and biomass burning, especially for years with extreme biomass smoke emissions, like 2012 (Kaskaoutis et al. 2014b), while the secondary peak in late pre-monsoon is attributed to the influence from dust aerosols coming from the west (Srivastava et al. 2011; Tiwari and Singh 2013). The monthly mean AOD_{500} and AE values at three wavelength ranges (i.e., shorter range 380–500 nm, mid-range 500–870 nm and long range 380–870 nm) are summarized in Table 2. The maximum AOD was observed in November (0.99 ± 0.30), while the minimum one in March (0.59 ± 0.19), which constitutes a transition period, without strong influence of dust (it usually starts from April onward). The maximum AOD_{500} in November is also associated with maximum AE values ($AE_{380–870} = 1.17 \pm 0.13$), indicating the dominance of the fine smoke aerosols. The minimum AE is observed in May ($AE_{380–870} = 0.69 \pm 0.19$), which suggests dominance of coarse-mode aerosols, with concurrent mixture of urban emissions. August and September are also characterized with lower AODs (~ 0.65–0.7) reflecting somewhat relatively clean atmospheric conditions due to

Table 1 Seasonal AOD_{500nm} and $AE_{380–870\ nm}$ at different places in Indo–Gangetic Basin and its surroundings

Location	Study period	AOD_{500nm}				$AE_{380–870nm}$				Reference
		W	Prm	M	PoM	W	Prm	M	PoM	
Varanasi	2011–2014	0.87	0.73	0.73	0.95	1.09	0.76	0.86	1.16	Present study
Varanasi	2011	0.90	0.67	0.68	0.78	1.11	0.70	0.72	1.2	Tiwari & Singh (2013)
GC**	2009		0.51–0.77				0.65–0.91			Srivastava et al. (2011)
GC**	2011		0.60–0.85				0.85–1.05			Tiwari and Singh (2013)
Kanpur	2001–2003	0.57	0.54	0.66	0.63	1.26	0.60	0.66	1.12	Singh et al. (2004)
Kanpur	2005–2010	0.63	0.59	0.60	.076	1.24	0.66	0.77	1.27	Kaskaoutis et al. (2012b)
Delhi	2011–2013	0.95	0.82	0.86	1.0	1.02	0.51	0.89	1.03	Tiwari et al. (2016a)
Delhi	2001–2012	0.77	0.78	0.74	0.91	0.97	0.49	0.66	0.93	Lodhi et al. (2013)
GN*	2010–2012	0.87	0.78	0.73	0.98	1.13	0.68	1.02	1.19	Sharma et al. (2014)
Jaipur	2011		0.50–0.80				0.38–0.60			Tiwari and Singh (2013)
Jodhpur	2004–2012	0.48	0.75	0.71	0.59	0.81	0.54	0.75	0.86	(Bhaskar et al. 2015)
Karachi	2010–2011	0.30–0.40	0.40–0.65			0.75–0.95	0.30–.40			Alam et al. (2012)
Lahore	2010–2011	0.63–0.76	0.55–0.75			1.0–1.25	0.40–0.60			Alam et al. (2012)
Ahmedabad	2002–2005	0.32	0.42	0.43	0.43	1	0.30	0.40	1.0	Ganguly et al. (2006)
Kharagpur	2009–2010	0.82	0.71			1.33	0.71			Pani and Verma (2014)
Kullu Valley	2006–2009	0.20	0.34	0.26	0.21	1.13	0.90	1.0	1.42	Guleria et al. (2012)
Nainital	2005–2008	0.11	0.30	0.15	0.09					Ram et al. (2010)
Gual Pahari	2009		0.64				0.53			Gautam et al. (2011)
Chitkara	2009		0.57				0.72			Gautam et al. (2011)
Goa	2008–2010			0.43						Shirodkar et al. (2015)
Pune	1998–2007	0.45	0.45		0.43	0.63	0.48			Dani et al. (2012)
Nagpur	2011	0.42	0.64	0.38	0.50	1.3	0.95	0.9	1.25	Kannemadugu et al. (2014)
Ananatpur	2007–2013	0.34	0.45	0.24	0.31	0.8–1.1		0.3–0.7		Reddy et al. (2016)
Hyderabad	2007–2008	0.55	0.65	0.60	0.46	1.06	1.02	0.58	0.89	Kaskaoutis et al. (2009)
Hyderabad	2008–2009	0.48	0.57	0.51	0.50	1.04	0.90	0.84	1.01	Sinha et al. (2013)
Dibrugarh	2001–2007	0.31	0.45	0.25	0.19	1.14	0.85	0.87	1.12	Gogoi et al. (2009)
Trivendrum	2002–2003	0.43	0.40	0.29	0.38	1.0	0.85	0.32	1.20	Moorthy et al. (2007)
Port Blair	2002–2008	0.31	0.26			0.93	1.1			Beegam et al. (2012)
AS##	1995–2002	0.29	0.47			0.70	0.30			Sateesh et al. (2006)
BoB#	2006–2012	0.26	0.44	0.41	0.27					Tiwari et al. (2016b)
AS##	2006–2012	0.24	0.34	0.77	0.33					Tiwari et al. (2016b)
Minicoy	1995–1998	0.32				1.12				Sateesh et al. (2002)

W winter, *Prm* pre-monsoon, *M* monsoon, *PoM* post-monsoon

*GN** Greater Noida, *GC*** Gandhi College, *BoB*# Bay of Bengal, *AS*## Arabian Sea

rainy washout during monsoon. For better understanding of the month-to-month variability in aerosols over Varanasi, the anomalies in AOD and AE from the respective monthly means are given in the Suppl. Fig. 2. The large anomaly values in both AOD (± 0.25) and AE (± 0.3–0.4) in certain months suggest a strong monthly mean variation along with seasonal variation in atmospheric turbidity and meteorological conditions. The seasonal mean spectral variation of AOD (Fig. 4b) reflects significant differences between the seasons. The spectral dependence of AOD values at UV–VIS wavelengths indicate the importance of the fine-mode aerosols in the scattering processes particularly during the post-monsoon and winter seasons (Sinha et al. 2013). Therefore, in spite of the very similar seasonal AODs at 870 nm (~ 0.5), post-monsoon and winter exhibit significantly larger AODs (~ 1.1–1.2) at the shorter wavelengths, which are attributed to the enhanced fine-mode aerosol scattering compared to the longer wavelengths (Kedia and Ramchandran 2011). The gradient between the spectral variability in AOD at shorter (340 nm) and longer (870 nm) wavelengths during the different seasons indicates the asymmetric distribution of the aerosol size distribution, i.e., seasonal changing effect on dominance of fine- and coarse-mode aerosols. The seasonal AODs and their

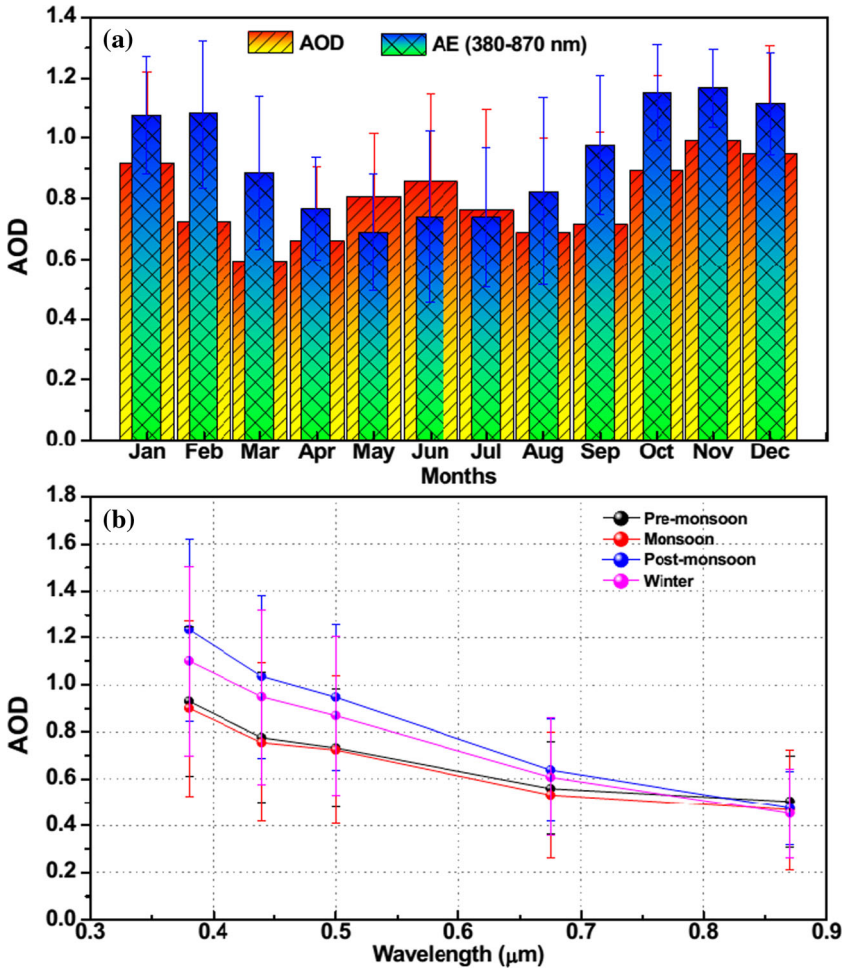

Fig. 4 Variation of the monthly mean AOD and AE (**a**) and the seasonal spectral means of AOD (**b**) over Varanasi during the study period (2011–2014)

wavelength dependence over Varanasi are similar to other studies over IGB (Lodhi et al. 2013; Sharma et al. 2014; Tiwari and Singh 2013; Tiwari et al. 2016a) as well as other locations in India (Kaskaoutis et al. 2009; Ramchandran 2007; Reddy et al. 2016).

Frequency distribution of AOD and AE

Figure 5 shows the frequency distribution of AOD_{500} and $AE_{380–870}$ for the four seasons, (a) pre-monsoon (Mar–Jun), (b) monsoon (Jul–Sep), (c) post-monsoon (Oct–Nov), and (d)

Table 2 Monthly mean ± 1σ value of AOD and AE during the study period over Varanasi

Months	AOD (380 nm)	AOD (500 nm)	AOD (870 nm)	AE (380–500 nm)	AE (500–870 nm)	AE (380–870 nm)
January	**1.16 ± 0.37**	0.92 ± 0.30	**0.48 ± 0.17**	0.87 ± 0.23	1.17 ± 0.21	1.08 ± 0.20
February	**0.94 ± 0.38**	0.72 ± 0.30	**0.39 ± 0.18**	0.98 ± 0.20	1.12 ± .032	1.08 ± 0.24
March	**0.76 ± 0.25**	0.59 ± 0.19	**0.37 ± 0.14**	0.90 ± 0.18	0.87 ± 0.34	0.89 ± 0.23
April	**0.85 ± 0.23**	0.66 ± 0.25	**0.45 ± 0.16**	0.90 ± 0.22	0.70 ± 0.20	0.77 ± 0.17
May	**1.02 ± 0.27**	0.81 ± 0.21	**0.58 ± 0.17**	0.83 ± 0.19	0.61 ± 0.27	0.69 ± 0.19
June	**1.08 ± 0.36**	0.86 ± 0.29	**0.60 ± 0.23**	0.86 ± 0.27	0.67 ± 0.38	0.74 ± 0.28
July	**0.92 ± 0.39**	0.76 ± 0.33	**0.53 ± 0.28**	0.73 ± 0.36	0.74 ± 0.36	0.74 ± 0.23
August	**0.84 ± 0.37**	0.69 ± 0.31	**0.47 ± 0.30**	0.78 ± 0.33	0.84 ± 0.46	0.83 ± 0.31
September	**0.90 ± 0.38**	0.72 ± 0.30	**0.42 ± 0.21**	0.89 ± 0.28	1.01 ± 0.34	0.98 ± 0.23
October	**1.18 ± 0.42**	0.89 ± 0.32	**0.46 ± 0.17**	1.04 ± 0.36	1.20 ± 0.29	1.15 ± 0.16
November	**1.27 ± 0.36**	0.99 ± 0.30	**0.49 ± 0.15**	0.92 ± 0.14	1.28 ± 0.19	1.17 ± 0.13
December	**1.19 ± 0.41**	0.95 ± 0.36	**0.48 ± 0.21**	0.86 ± 0.18	1.24 ± 0.18	1.12 ± 0.17

winter (Dec–Feb). The seasonal mean AOD and AE along with $\pm 1\sigma$ and the total number of scans (N) in each season are also given in the corresponding graphs. A large range in both AOD and AE distributions is observed for all seasons indicating a significant variability in aerosol types and their size distribution due to various emission sources and seasonally changed meteorological conditions. The results reveal a significant frequency for higher AODs (> 0.7) reaching to 49, 45, 76, and 64% in pre-monsoon, monsoon, post-monsoon, and winter, respectively, indicating highly turbid atmospheric conditions throughout the year. On the other hand, lower values of AE (< 0.6) are found during the pre-monsoon and monsoon seasons (21 and 19%, respectively), suggesting a larger contribution of coarse-mode particles over Varanasi, while this fraction becomes negligible (nearly 1.5%) during post-monsoon and winter. A unimodal frequency distribution is observed for both AOD and AE values during all the seasons, but with different modal values, which are close to 0.8 for the AOD in all seasons except monsoon (0.6). However, the AE distributions exhibit very contrary modal values,~ 1.2 for post-monsoon and winter and 0.8 for pre-monsoon. During the pre-monsoon season, the AOD values vary widely between 0.4 and 1.8, while the AE exhibits a similar range of 0.4–1.4, with mean values of 0.73 ± 0.25 for AOD_{500} and 0.76 ± 0.23 for the $AE_{380–870}$, respectively. The highest frequency (30–37%) is observed in the range of 0.7–0.9 for both AOD and AE during pre-monsoon. During monsoon, the AOD_{500} is somewhat shifted to lower values, with the highest frequency around 0.6 and a progressive decrease afterwards. The AE values are slightly shifted towards higher values with maximum frequency around 1.0, characteristic of well mixing atmospheric conditions and similar contributions of fine and coarse particles (Eck et al. 2005). In contrast, during the post-monsoon and winter seasons, although the AOD_{500} has similar distributions between 0.4 and 2.0 with maximum frequency around 0.8, the AE is strongly shifted to larger values with ~ 70–90% of the values lying in the range of 1.2–1.4, suggesting enhancement of the fine particles and similar aerosol emission sources, i.e., anthropogenic combustion and biomass burning.

Aerosol properties and modification processes

Figure 6 shows the scatter plots between the coefficient A_2 obtained from the second-order polynomial fit (Eq. 2) and the AOD_{500} in each season, while the color scale represents the $AE_{380–870}$. The coefficient A_2 expresses the curvature of the polynomial fit and has been extensively used for better characterization of the aerosol properties and the dominance between fine and coarse modes (Eck et al. 1999; Kaskaoutis et al. 2007; Schuster et al. 2006). Therefore, the correlation between A_2 and AOD could be used to discriminate different aerosol types and provide vital information about their physical properties (like volume fraction and effective radius) for different AE values (Schuster et al. 2006). Values of $A_2 \approx 0$ correspond to negligible curvature and to aerosol size distributions following the Junge power law (i.e., unimodal size distribution) (Eck et al. 1999; Kaskaoutis et al. 2009). The curvature is found to be mostly positive during the pre-monsoon season associated with moderate-to-low AE values (mostly below 0.9) and in many cases high (> 1.0) AODs (Fig. 6a), suggesting bimodal size distributions with dominance of the coarse mode (Eck et al. 1999; Schuster et al. 2006). However, for the highest AODs, there is a tendency of the A_2 to approach zero, as was also found over turbid desert environments, like Solar Village (Kaskaoutis et al. 2007). Therefore, this seems to be a characteristic for the coarse-mode particles under very turbid environments, i.e., weakening of the curvature and the flat spectral dependence of the AOD, with AE values near to zero. On the other hand, some data points in pre-monsoon that are characterized by high AODs (~ 0.8–1.2) and AE values above 1.0, exhibit negative curvatures suggesting bimodal size distributions with high or even dominance of the fine-mode aerosols, mostly originating from urban emissions, agricultural burning of wheat residue and forest fires in the Himalayan foothills (Kumar et al. 2011; Vadrevu et al. 2012). Previous studies have also reported bimodal size distributions and existence of biomass-burning aerosols during pre-monsoon over various sites in IGB (Ram et al. 2016; Srivastava et al. 2011; Tiwari and Singh 2013). In contrast, mostly negative values of the coefficient A_2 are shown in post-monsoon and winter, especially for the higher values of AOD and AE. This suggests dominance of fine-mode aerosols that express larger AE values at the longer rather than shorter wavelengths and negative curvatures, while the opposite exists in the case of desert dust (Eck et al. 1999; Schuster et al. 2006). This is consistent with the findings by Kaskaoutis et al. (2014b), who reported dominance of fine-mode aerosols due to biomass/crop residue burning over the entire IGB (Varanasi site also included) during the post-monsoon season. However, for lower AOD values, a wide range and several cases of positive A_2 are also observed, which are associated with mixed aerosol state and/or coagulation processes in the atmosphere that increased the particle size and the coarse-mode fraction. It should be also noted that these cases are associated with a larger degree of uncertainty in the A_2 retrievals, as shown in Fig. 2. Similarly, relatively lower AE values are associated with lower AOD and small positive curvature during the winter season suggesting a possibility of increase in the fine-mode size through coagulation/condensation processes. Similar results are also observed at several IGB sites (e.g., Patiala, Delhi, Varanasi, Kanpur, Gandhi College) during the late pre-monsoon and winter (Gobbi et al. 2007; Kaskaoutis et al. 2014b), as well as in Hyderabad (Sinha et al. 2012) and Bay of Bengal (Kaskaoutis et al. 2011). Except of the lower values of the

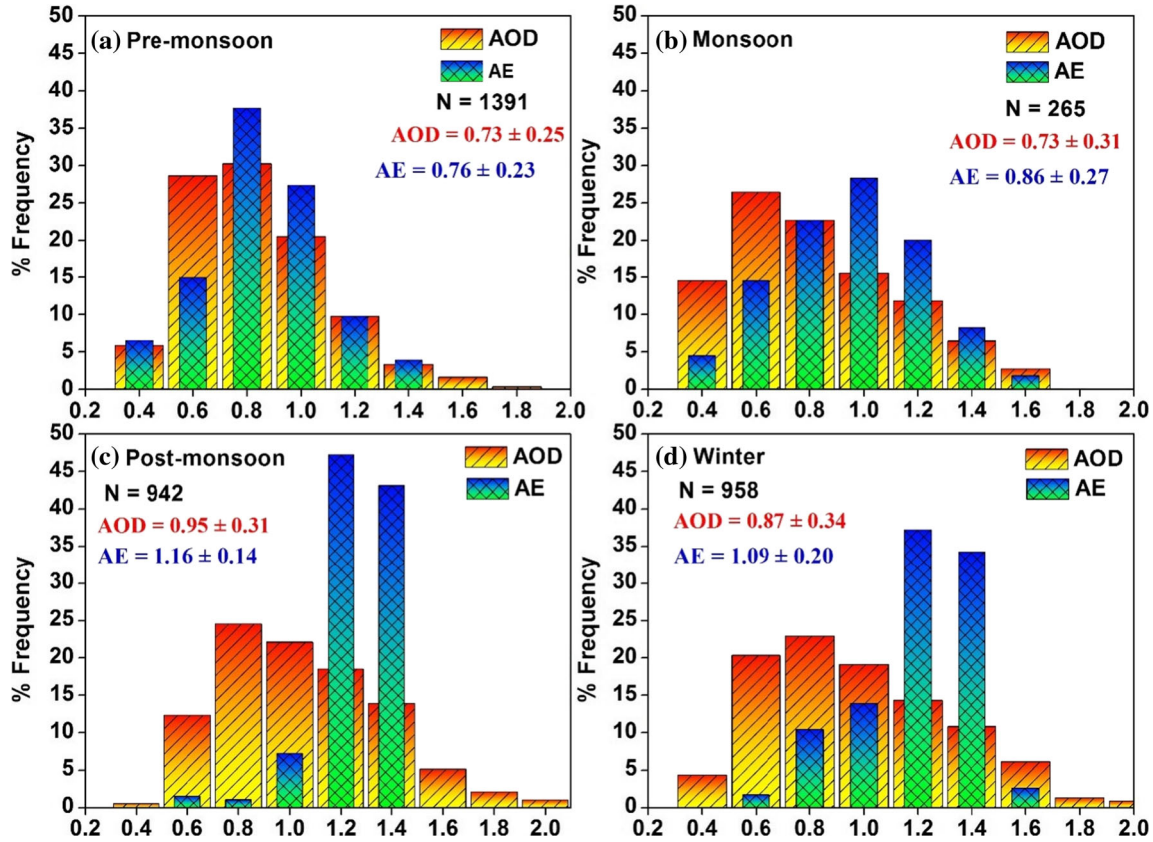

Fig. 5 Seasonal frequency distributions of the AOD and AE values over Varanasi during the study period. The total number of scans in each season is given by 'N',while the seasonal mean AOD and AE values with ± 1σ are also given

$AE_{380–870}$ during pre-monsoon and monsoon, the AEs at short wavelengths (e.g., 380–500 nm) were found to be significantly larger than the respective AE values at mid-range wavelengths (e.g., 500–870 nm), while the opposite exists in post-monsoon and winter, indicating seasonally changed dominance of aerosols of different origin, type, size, and composition within a year-round turbid urban environment.

The wavelength dependence of the AE has been successfully used for the characterization and identification of different aerosol types as well as for examining the modification processes in the atmosphere. The AE value computed at shorter wavelengths gives useful information about changes in the fine-mode particle size, while at longer wavelengths, it provides valuable information about variations in the fine-to-coarse-mode ratio (Kaskaoutis et al. 2007; Reid et al. 1999; Schuster et al. 2006; Tiwari et al. 2016a). In this respect, Gobbi et al. (2007) proposed a simple graphical method to classify the aerosol types and examined the contribution of the fine mode to the modification processes in the atmosphere under increasingly turbid environments using the correlation between $AE_{440–870}$ and the difference in AE (dAE) between 440–675- and 675–870-nm bands (i.e., $dAE = AE_{440–675} – AE_{675–870}$) for various fine-mode radius (R_f) and fine-mode fractions (η). The classification scheme is totally based on the Mie scattering and correlates the fine-mode fraction at 675 nm and the effective radius of fine-mode aerosols for increasing AOD groups. Negative values of dAE are associated with negative curvature suggesting dominance of fine-mode aerosols and vice versa**.** Since, AE and dAE both are derived from AOD value, a lower value of AOD (≤ 0.10) results to an error in AE and dAE of $\geq 20\%$ and $\geq 50\%$ respectively (Gobbi et al. (2007). Therefore, in order to minimize any possible uncertainties, in the present analysis, the whole set of observation having an AOD value greater than 0.15 (AOD > 0.15) is used. More details about the classification scheme and sensitivity analysis are discussed in Gobbi et al. (2007).

Figure 7 represents the variation of dAE between shorter and longer wavelengths against the broadband $AE_{440–870}$ as a function of AOD_{500} during (a) pre-monsoon, (b) monsoon, (c) post-monsoon, and (d) winter seasons. The black lines indicate the effective radius (R_f) of the fine mode and the blue lines the fixed percentage fraction ($\eta\%$) of the fine mode, while the colored spheres with increasing size represent the increasing AOD_{500}. In general, a large variation in both AE and dAE is observed associated with a wide range of AOD in all seasons, indicating significant heterogeneity in aerosol types with a mixture of fine- and coarse-mode aerosols, as discussed in the previous analysis. On some days, mostly in pre-monsoon, the data points lie outside the graphical scheme, which may be attributed to larger refractive index. Especially

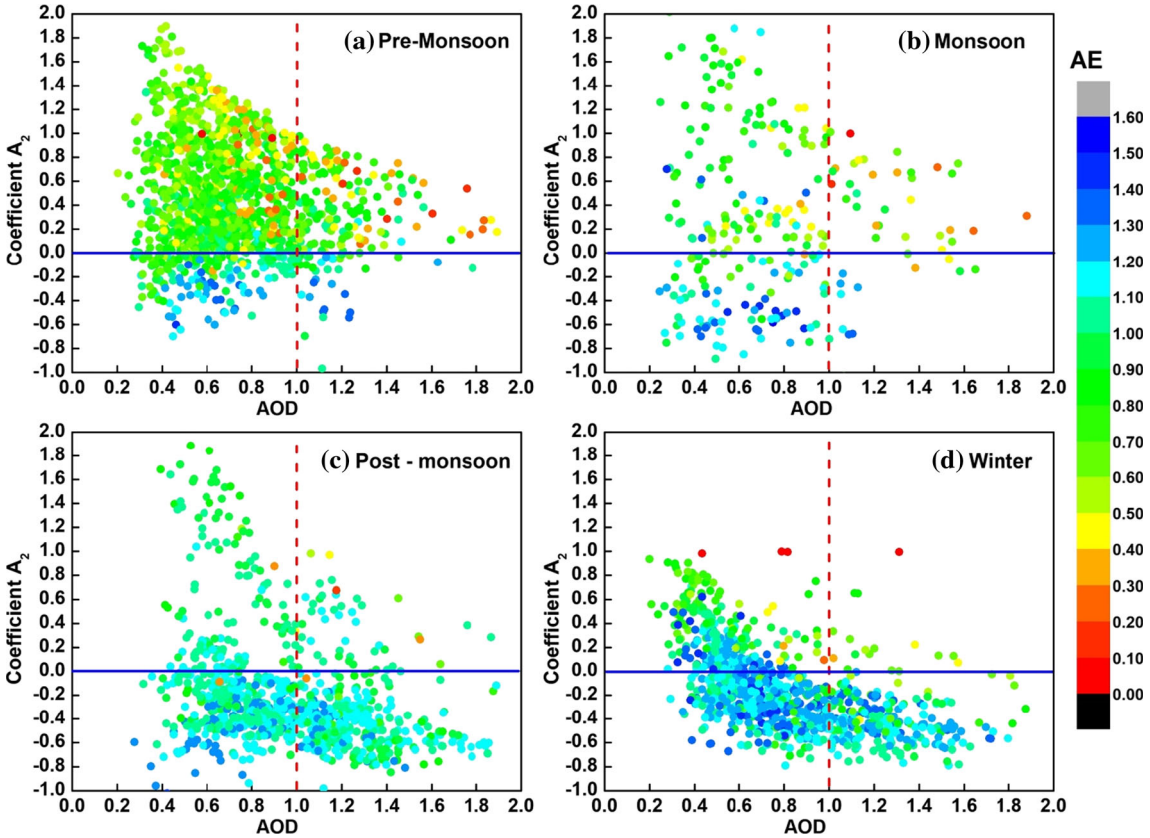

Fig. 6 Scatter plot between AOD and curvature coefficient A_2 as a function of AE (colored scale) during **a** pre-monsoon, **b** monsoon, **c** post-monsoon, and **d** winter seasons

in the pre-monsoon period, the high positive values of dAE for lower AE values indicate large curvatures and significant higher AE at shorter wavelengths characteristic of non-spherical desert dust particles (Reid et al. 1999). Therefore, the positive curvature is mostly observed for higher AOD (> 0.8) and lower (< 0.6) AE values, underlying the influence of desert dust with low (< 30%) fine-mode fraction. Negative dAE values are observed in very few cases under moderate-to-low AODs, suggesting large contribution of urban anthropogenic emissions in the absence of dust plumes. The increasing AOD does not exhibit a clear shift of the data points towards lower or higher R_f, but it suggests that the higher aerosol loading in pre-monsoon is due to the presence of dust plumes, leading to lower fine-mode fraction. However, on few days, the highest AOD values are associated with values of AE above 1.0, suggesting the abundance of crop residue burning or smoke from forest fires, as they are associated with $\eta >$ 50–60%. Several previous studies have also reported the dominance of dust and influence of biomass-burning aerosols on certain circumstances over IGB during the pre-monsoon season (Gautam et al. 2009; Pandithurai et al. 2008; Srivastava et al. 2011; Sharma et al. 2012; Singh and Beegum 2013; Tiwari el al. 2013; Singh et al. 2016).

In the monsoon season, the scatter plot between AE and dAE is totally different than the other seasons. The much fewer data points due to cloudy-rainy conditions and the large scatter provide inconclusive results about the aerosol modification processes, but a general shift towards a lower η and positive dAE is observed as AOD increases. Furthermore, there is a slight shift towards the origin of the graphical scheme, suggesting an increase in concentrations of coarse-mode particles after hygroscopic growth (hydration processes) (Ferrare et al. 2000; Gobbi et al. 2007). A shift towards the origin was also reported over the humid environment of the Arabian Sea (Kaskaoutis et al. 2010) and over Hyderabad in monsoon (Sinha et al. 2012). In contrast, very different scatter patterns are observed in post-monsoon and winter, since the highest AODs (> 0.8) are associated with larger fine-mode fractions (> 70%) and AE (> 1.0). The results suggest the dominance of fine-mode aerosols of combustion origin (e.g., fossil fuels, biomass burning, crop residue burning). Similar features for the aerosol modification processes over Varanasi were reported during the post-monsoon of 2012, which is characteristic of the enhancement in fine-mode aerosols due to biomass/crop residue burning and coagulation processes under very turbid urban environments (Kaskaoutis et al. 2014b). During winter, the change from low to high AODs exhibits a shift towards larger R_f values (from 0.10to 0.20 μm), which is characteristic of condensation and coagulation processes of urban aerosols under turbid environments,

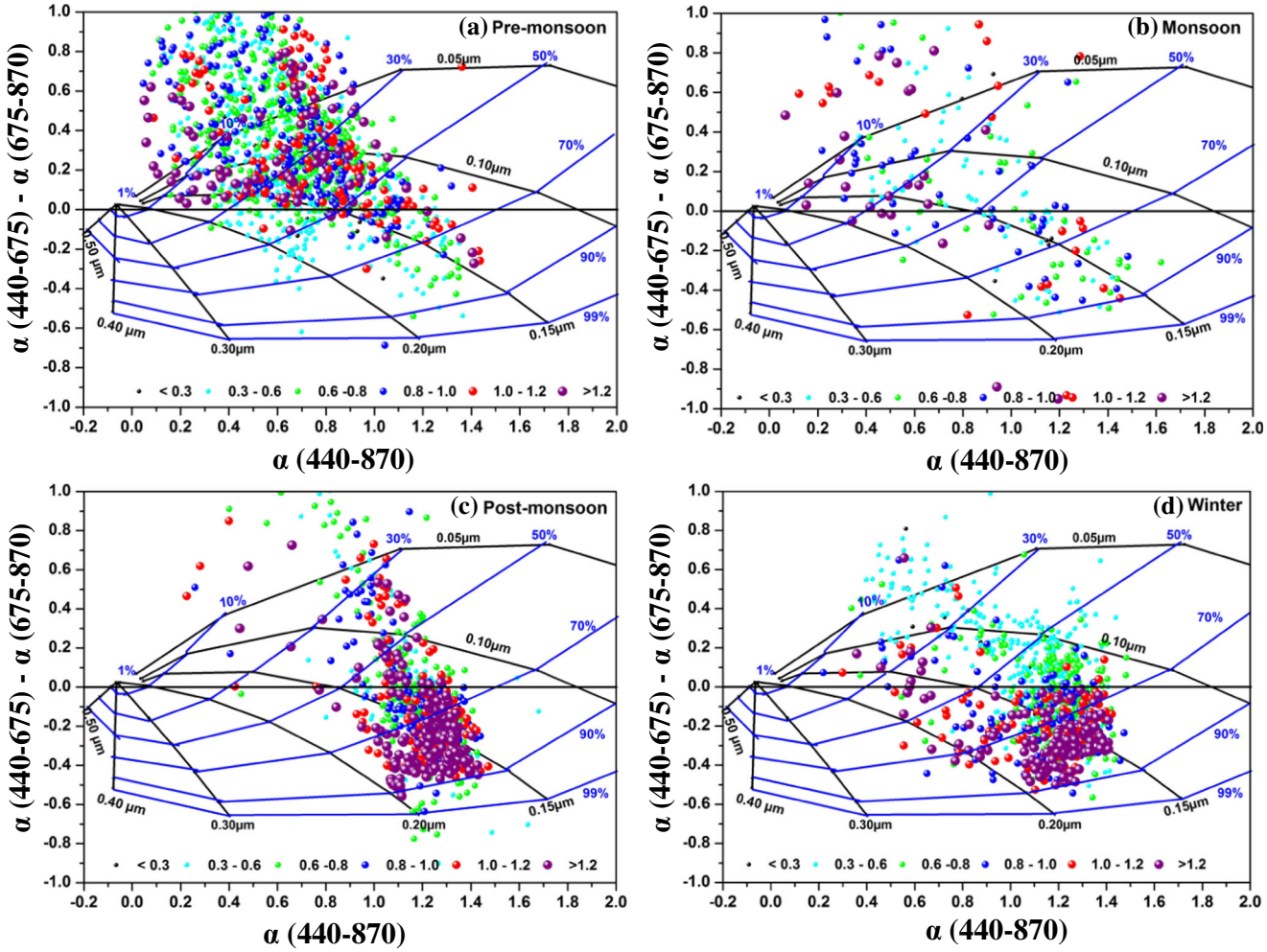

Fig. 7 Variation of the Angstrom exponent difference [AE(440–675 nm) − AE(675–870 nm)], as a function of the AE (440–870 nm) and AOD_{500} (in colored scale) over Varanasi, for bimodal log-normal size distribution during **a** pre-monsoon, **b** monsoon, **c** post-monsoon, and **d** winter seasons. The black lines indicate the fixed effective radius of the fine mode (R_f) and the blue lines the fixed fraction of fine mode to the AOD (η)

and a significant increase (from ~ 50 to ~ 90%) in η. The same feature was also shown over other polluted urban environments like Kanpur, Beijing (Gobbi et al. 2007), Greater Noida (Sharma et al. 2014), Hyderabad (Sinha et al. 2012), and over the Bay of Bengal due to intense continental pollution outflow during winter (Kaskaoutis et al. 2011). On the other hand, slight positive dAE values for high AODs and $AE_{440–870}$ around 0.6 in winter correspond to aged smoke plumes with larger sizes of R_f, while the η below 50% indicates mixing with road re-suspended dust within the urban environment.

Aerosol-type classification

Previous analysis showed that Varanasi experiences a mixture of aerosol types with very different optical properties and size distribution along the seasons. Therefore, for better understanding of the aerosol characteristics, a classification of their types and apportionment of their emission sources are needed. Different researchers have followed various classification techniques for the aerosol-type identification based on the correlation between absorption and extinction Angstrom exponents (Giles et al. 2011; Russell et al. 2010), on the correlation between single scattering albedo and fine-mode fraction (Lee et al. 2010; Tiwari et al. 2015b), on the wavelength dependence of single scattering albedo (Eck et al. 1999) and the correlation between AOD and AE (Kaskaoutis et al. 2009; Tiwari et al. 2016a). In this study, we used a scatter plot between AOD and AE (Fig. 8) to classify different aerosol types over Varanasi. Based on threshold values for AOD and AE from literature, five dominant aerosol types were identified, i.e., Mostly dust (MD), polluted continental (PC; dominant anthropogenic aerosols with dust), anthropogenic aerosol (AA; mainly coming from urban/industrialized regions around the measuring site, as well as from vehicular emissions), biomass burning (BB; mainly coming through biomass/crop residue burning in the

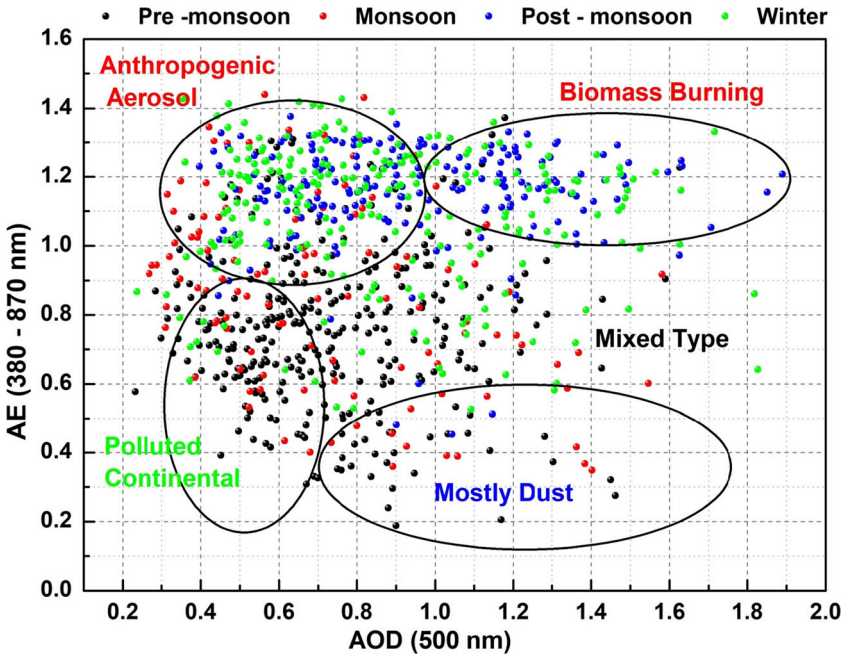

Fig. 8 Scatter plot between AOD_{500} vs $AE_{380–870}$ for discrimination of different types of aerosols over Varanasi on seasonal basis

IGB), and mixed type (MT) aerosol. More specifically, the MD type is associated with high AOD (> 0.7) and AE values less than 0.6; PC has relatively higher AE (AE < 0.9) with AOD values in the range of 0.3–0.7. Higher values of AE (AE > 0.9) with a wide range of AOD (0.3–1.0) represent the AA type and the cases with very high AOD and AE, both above 1.0, correspond to the BB aerosol type. The cases that do not belong to any of the above mentioned categories are inferred as MT aerosols. To understand the size dominance in individual inferred aerosol particles, curvature coefficient (A_2) is plotted against AOD (Fig. 9). The results suggest that the MD and PC aerosol types have mostly positive curvature indicating relative dominance of coarse-mode aerosol particles, while the BB aerosols exhibit negative curvature indicative of the dominance of fine-mode particles. Apart from this, the MT and AA types have both positive and negative curvatures suggesting a mixture of fine as well as coarse-mode aerosols over the urban environment. The percentage contribution of each aerosol type on seasonal and annual basis is shown in Fig.10. The analysis reveals that during pre-monsoon, the aerosols over Varanasi are mostly of PC type (≈ 40%) and MT (≈ 25%) due to the strong influence of dust plumes transported from the Thar Desert or even Arabia mixed with urban emissions. The AA type has maximum contribution during post-monsoon and winter (≈ 56%) followed by monsoon (≈ 41%).The BB aerosol type is more frequent during post-monsoon (≈ 37%) and winter (≈ 22%) due to extensive crop residue burning over northwestern IGB and less influence of other natural aerosols. The BB type has negligible contribution during the pre-monsoon and monsoon seasons; despite the several forest fires in the Himalayan foothills and the agricultural burning in central India, as these aerosols are mixed with desert dust or road dust re-suspension within the urban environment in pre-monsoon. A small fraction (≈ 13%) of MD aerosols also contributes in aerosol loading during pre-monsoon and monsoon, which reduces on an annual basis (≈ 7% only). The analysis shows that in post-monsoon and winter seasons, the atmospheric conditions seem to be dominated by fine particles and mostly composed of carbonaceous aerosols, sulfates, and nitrates from urban/industrial emissions (e.g., power plants, vehicle emissions, brick kilns) and biomass burning (bio-fuel, wood and waste material burning for cooking and heating, agricultural crop-residue burning) (Habib et al. 2008; Li et al. 2017; Ram et al. 2010; Rehman et al. 2011; Tiwari et al. 2015a). On an annual basis, the AA type exhibits maximum frequency (≈ 41%), followed by PC (≈ 19%), MT (17%) and BB (16%) indicating a dominance of fine-mode aerosols on a yearly basis.

Transport pathways and source apportionment

In order to identify the distant emission sources and trajectory pathways for the various aerosol types, 5-days air mass back trajectories ending at 1000 m above the ground level were computed using the HYSPLIT model. The air mass back trajectories provide significant information about the emission sources of air pollutants and their transport pathways to the measurement sites. Aerosol loading and their composition at any location are highly influenced by the meteorological parameters over particular region which affect the air mass transport. The daily 5-day air mass back trajectories from NOAA-HYSPLIT (National Oceanic and Atmospheric Administration Hybrid Single-Particle Lagrangian Integrated Trajectory) model were analyzed (Draxler and Rolph 2003) at Varanasi. It provides a three-dimensional (latitude,

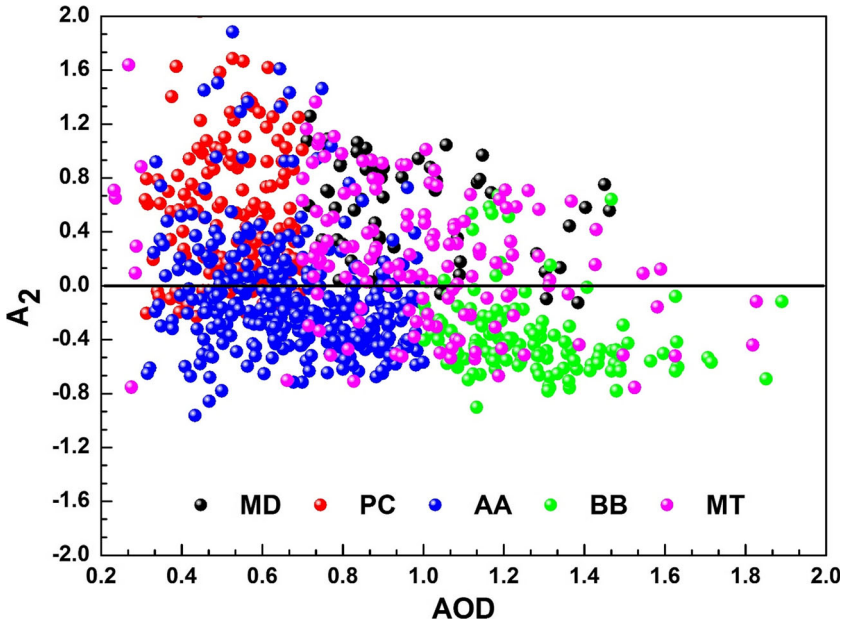

Fig. 9 Scatter plot between the curvature coefficient (A_2) and AOD_{500} for the inferred aerosol types (BB: biomass burning; AA: anthropogenic aerosol; MT: mixed type; PC: polluted continental; and MD: Mostly Dust) over Varanasi

longitude, and altitude) description of the pathways followed by air masses as a function of time by using National Centre for Environmental Prediction (NCEP) reanalysis wind database as input to the model. Although these back trajectories could define the transported pathways of aerosols, are unable to effectively delineate the potential aerosol source regions (Vaughan et al. 2002; Gogoi et al. 2011). Therefore, an additional statistical analysis, i.e., the potential source contribution function (PSCF), is used to evaluate the contribution of the emission sources. This technique is well accepted in examining the aerosol and pollutants source apportionment and widely used throughout the world (Kulshrestha et al. 2009; (Dimitriou and Kassomenos 2016; Ding et al. 2017; Gogikar and Tyagi 2016; Ming et al. 2017; Raman and Ramachandran 2011; Vaishya et al. 2017; Xin et al. 2016; Yao et al. 2016; Zheng et al. 2017)). It represents the conditional probability of potential direction of pollution sources and the contribution of grid cells. The PSCF values for the grid cells are calculated by counting the trajectory segment endpoints that terminate within each cell and given by:

$$\mathrm{PSCF}_{ij} = m_{ij}/n_{ij} \tag{3}$$

where m_{ij} represents the number of end points of a pollution trajectory traversing the grid (i,j) and n_{ij} represents the total

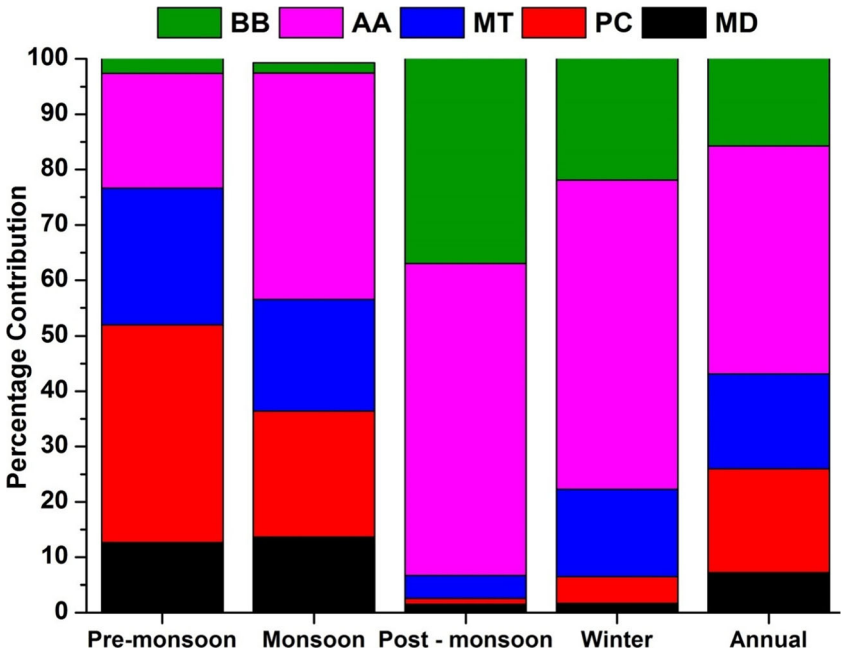

Fig. 10 Percentage contribution of the different aerosol types (BB: biomass burning; AA: anthropogenic aerosol; MT: mixed type; PC: polluted continental; and MD: mostly dust) over Varanasi on seasonal and annual basis

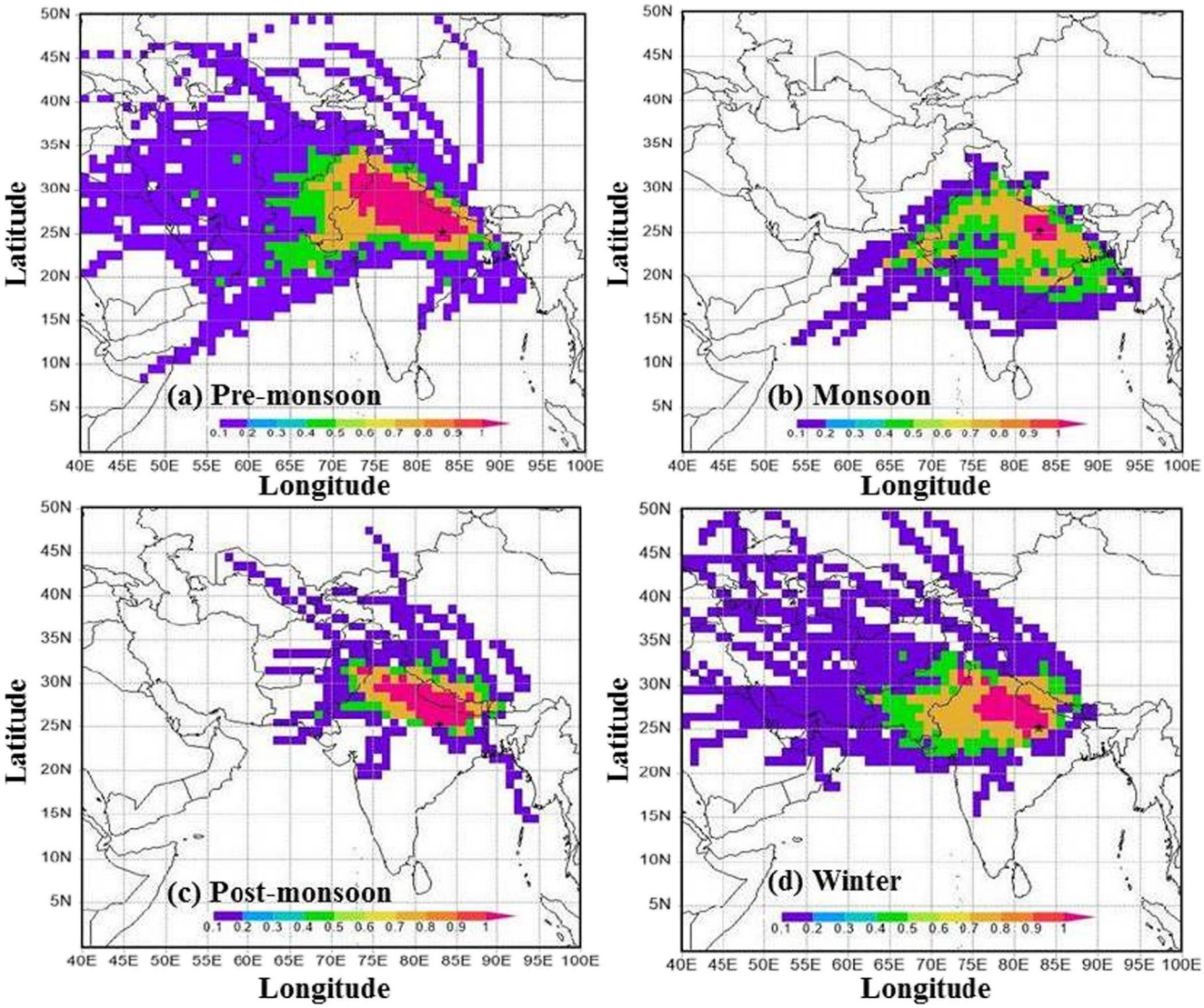

Fig. 11 Weighted Potential Source Contribution Analysis (WPSCF) plots of 5 days air mass back trajectories at Varanasi during **a** pre-monsoon, **b** monsoon, **c** post-monsoon, and **d** winter seasons

number of endpoints of all trajectories falling within the grid (i, j), while i and j represent the longitude and latitude, respectively. Higher PSCF values indicate larger potential contributions of the pollutant concentration at the receptor site, while the trajectories passing these cells represent the major transport pathways leading to the high pollutant loadings at the receptor site. In the present study, the experimental area (Indian subcontinent) is divided into $1^{\circ} \times 1^{\circ}$ grid. Since PSCF is a kind of conditional probability, the error increases with increases in the distance between grid and sample points. Therefore, to reduce this uncertainty, PSCF is multiplied by the weighting function which is given by:

$$W_{ij} = \begin{cases} 1.00 & 80 < n_{ij} \\ 0.70 & 20 < n_{ij} \leq 80 \\ 0.42 & 10 < n_{ij} \leq 20 \\ 0.05 & n_{ij} \leq 10 \end{cases} \quad (4)$$

In order to reveal the differences in air mass trajectories and the possible aerosol hot-spot areas during the different seasons over Varanasi, the weighted PSCF (WPSCF) analysis for AOD is performed on seasonal basis (Fig. 11). The colored scale represents the contribution of the aerosol emission sources. The northwestern IGB and the Thar desert have the maximum contributions during pre-monsoon, thus suggesting a mixture of dust with pollutants and wheat crop residue burning on this season (Kumar et al. 2011). Furthermore, long-range transported dust plumes from Arabia, Middle East, and southwest Asia are also favored during pre-monsoon and in a much-limited scale in monsoon. Except for the IGB sources, Varanasi may be also influenced by marine air masses from the Arabian Sea and Bay of Bengal during monsoon, while the rainfall contributes to washout of the distant aerosols and pollutants, leading to local

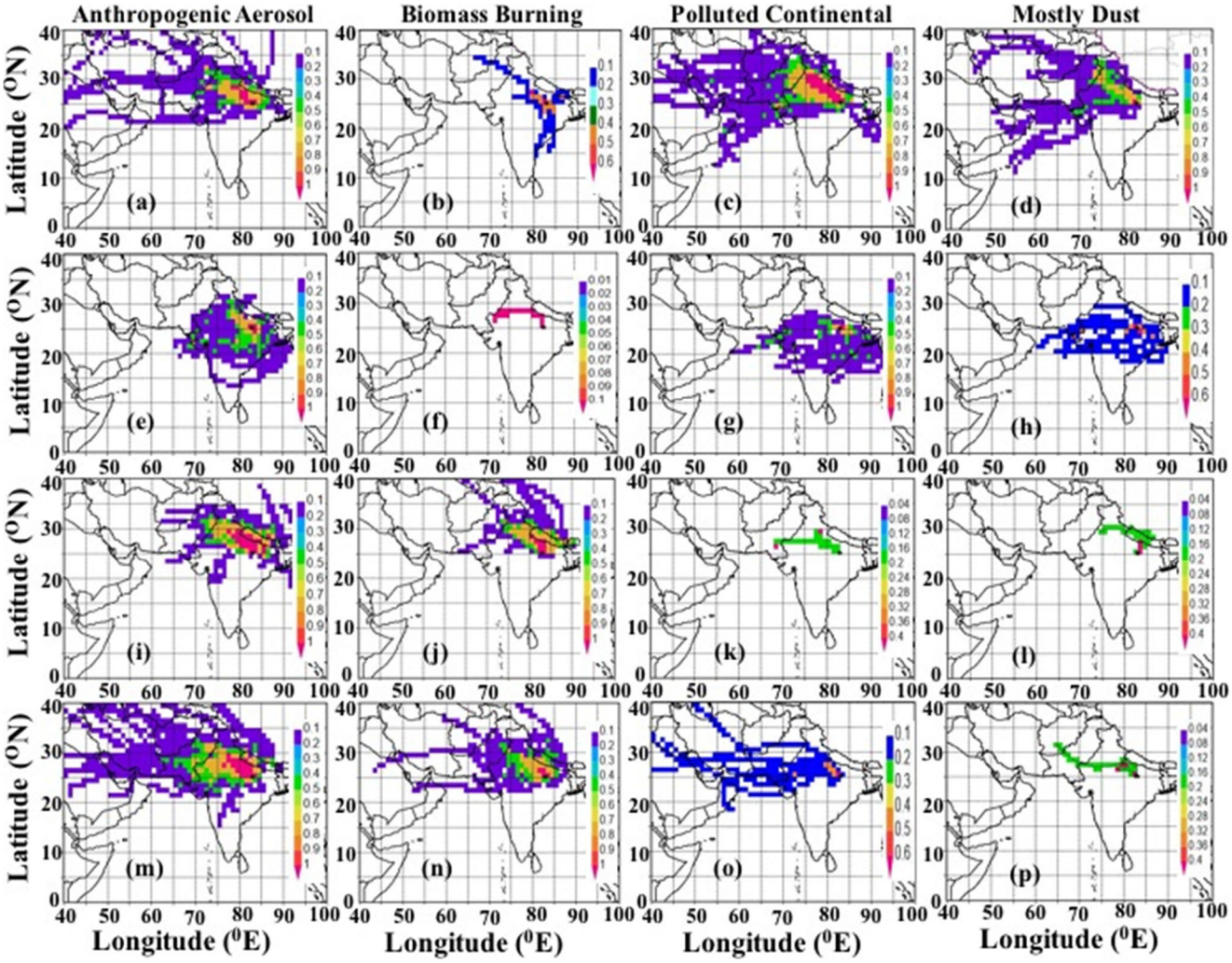

Fig. 12 Weighted Potential Source Contribution Analysis (WPSCF) plots of 5 – days air mass back trajectories for the different aerosol types during pre-monsoon (**a–d**), monsoon (**e–h**), post-monsoon (**i–l**), and winter (**m–p**) seasons

contributions for the high AODs. On the other hand, during post-monsoon, the aerosol sources are much more limited over the IGB and Varanasi is mostly influenced by the northwestern India, where significant paddy crop residue burning occurs in this season (Kaskaoutis et al. 2014b; Rajput et al. 2014). During winter, the air masses are mostly coming from northwestern directions, carrying similar types of aerosols as in post-monsoon. There is also possibility of long-range transported plumes from Arabia and southwest Asia, which, however, are not so enriched in dust due to low dust activity over these areas in winter (Rashki et al. 2014). Furthermore, in order to determine the possible emission sources of the inferred aerosol types over Varanasi, the WPSCF was also performed for the individual aerosol types on seasonal basis (Fig. 12). The figure shows that the AA type mainly comes from local emission sources; however, relatively smaller contribution of AA aerosols is also observed through transportation during pre-monsoon and winter seasons. The BB aerosols mainly originate from local sources during pre-monsoon, while in post-monsoon and winter seasons, northwestern India exhibits the maximum contribution over Varanasi for this aerosol type. The sources for the PC aerosol type show similarities with those for the AA type with higher WPSCF values over northwestern India, while a smaller contribution is also found for long-range transport during the pre-monsoon and winter seasons. The MD type exhibits maximum WPSCF values near the arid western part of India, while in certain cases, potential sources from southwest Asia (Pakistan, Afghanistan) and southeastern Arabia are shown, indicating significant contribution to dust aerosols through long-range transport. The WPSCF analysis highlights the different emission sources and hot-spot areas for the different aerosol types over Varanasi, also indicating the seasonally changed emission potentials between anthropogenic and natural aerosols that are accumulated over the IGB throughout the year.

Conclusions

Continuous MICROTOPS-II sun-photometer measurements were carried out at Varanasi, located in the central IGB, for 4 years (January 2011 to December 2014) in order to examine the columnar aerosol characteristics, the inter-/intra-seasonal variability, the dominant aerosol types, and source regions. The key findings of the present study can be summarized as follows:

1. Significant heterogeneity in aerosol loading and properties was observed over Varanasi with a strong inter/intra seasonal variability exhibiting maximum AOD (0.95 ± 0.31) and AE (1.16 ± 0.14) during the post-monsoon season.
2. The frequency distributions of AOD and AE were found to be unimodal during all seasons except monsoon with different modal values.
3. A considerable curvature in the spectral variation of AOD was observed, which was associated with higher values of AOD and AE during the post-monsoon and winter seasons indicating dominance of fine-mode aerosols.
4. Five different aerosol types were identified over Varanasi, which showed a remarkable seasonal variation in their contribution. Post-monsoon and winter seasons were dominated by anthropogenic and biomass-burning aerosols, whereas the polluted continental and mixed types were more frequent in pre-monsoon.
5. Source-apportionment analysis showed that the northern India had major contribution in aerosol loading over Varanasi, mostly for the anthropogenic and biomass-burning aerosols, while the dust particles might also have reached via long-range transport which originate from distant sources (Arabia and southwest Asia).

Further analysis in aerosol properties and estimates of the aerosol radiative effects is needed for better understanding of their role in climate implications over northern India.

Acknowledgements We acknowledge NOAA HYSPLIT model for back-trajectory analysis. The authors are grateful to the two anonymous reviewers for their constructive comments and suggestions to improve the manuscript.

Funding information This study is partially supported by ISRO under the ISRO SSPS program and partially by UGC, New Delhi, under the MRP Program. First author, S. Tiwari, is thankful to the Council of Scientific and Industrial Research (CSIR) for providing a senior research fellowship.

References

Alam K, Trautmann T, Blaschke T, Majid H (2012) Aerosol optical and radiative properties during summer and winter seasons over Lahore and Karachi. Atmos Environ 50:234–245

Altaratz O, Koren I, Remer LA, Hirsch E (2014) Review: cloud invigoration by aerosols—coupling between microphysics and dynamics. Atmos Res 140-141:38–60

Angstrom A (1964) The parameters of atmospheric turbidity. Tellus 16: 64–75

Babu SS, Manoj MR, Moorthy KK, Gogoi MM, Nair VK, Kompalli SK, Satheesh SK, Niranjan K, Ramagopal K, Bhuyan PK, Singh D (2013) Trends in aerosol optical depth over Indian region: potential causes and impact indicators. J Geophys Res 118:11,794–11,806

Badarinath KVS, Kharol SK, Sharma AR (2009) Long-range transport of aerosols from agriculture crop residue burning in Indo–Gangetic plains—a study using LIDAR, ground measurements and satellite data. J Atmos Sol Terr Phys 71:112–120

Beegum SN, Moorthy KK, Babu SS, Satheesh SK, Vinoj V, Badarinath KVS, Safai PD, Devara PCS, Singh S, Vinod, Dumka UC, Pant P (2009) Spatial distribution of aerosol black carbon over India during pre-monsoon season. Atmos Environ 43:1071–1078

Beegum SN, Moorthy KK, Gogoi MM, Babu SS, Pandey SK (2012) Multi-year investigations of aerosols from an island station, Port Blair, in the Bay of Bengal: Climatology and source impacts. Ann Geophys 30:1113–1127

Bhaskar V, Safai PD, Raju MP (2015) Long term characterization of aerosol optical properties: implications for radiative forcing over the desert region of Jodhpur, India. Atmos Environ 114:66–74

Bonasoni P, Laj P, Marinoni A, Sprenger M, Angelini F, Arduini J, Bonafè U, Calzolari F, Colombo T, Decesari S, di Biagio C, di Sarra AG, Evangelisti F, Duchi R, Facchini MC, Fuzzi S, Gobbi GP, Maione M, Panday A, Roccato F, Sellegri K, Venzac H, Verza GP, Villani P, Vuillermoz E, Cristofanelli P (2010) Atmospheric brown clouds in the Himalayas: first two years of continuous observations at the Nepal Climate Observatory-Pyramid (5079 m). Atmos Chem Phys 10:7515–7531

Dani KK, Ernest Raj P, Devara PCS, Pandithurai G, Sonbawne SM, Maheskumar RS, Saha SK, Jaya Rao Y (2012) Long-term trends and variability in measured multi-spectral aerosol optical depth over a tropical Urban Station in India. Int J Climatol 32:153–160

Das SK, Jayaraman A, Misra A (2008) Fog-induced variations in aerosol optical and physical properties over the Indo-Gangetic Basin and impact to aerosol radiative forcing. Ann Geophys 26:1345–1354

Dey S, Di Girolamo L (2010) A climatology of aerosol optical and microphysical properties over the Indian subcontinent from 9 years (2000–2008) of Multiangle Imaging Spectroradiometer (MISR) data. J Geophys Res 115:D15204. https://doi.org/10.1029/2009JD013395

Dey S, Tripathi SN, Mishra SK (2008) Probable mixing state of aerosols in the Indo-Gangetic Basin, northern India. Geophys Res Lett 35: L03808. https://doi.org/10.1029/2007GL032622

Dimitriou K, Kassomenos P (2016) Combining AOT, Angstrom Exponent and PM concentration data, with PSCF model, to distinguish fine and coarse aerosol intrusions in Southern France. Atmos Res 172–173:74–82

Ding X, Kong L, Du C, Zhanzakova A, Wang L, Fu H, Chen J, Yang X, Cheng T (2017) Long-range and regional transported size-resolved atmospheric aerosols during summertime in urban Shanghai. Sci Total Environ 583:334–343

Draxler RR, Rolph GD (2003) HYSPLIT (Hybrid single-particle Lagrangian integrated trajectory) model. NOAA Air Resources Laboratory, Silver Spring

Dumka UC, Tripathi SN, Misra A, Giles DM, Eck TF, Sagar R, Holben BN (2014) Latitudinal variation of aerosol properties from Indo-Gangetic Plain to central Himalayan foothills during TIGERZ campaign. J Geophys Res Atmos 119:4750–4769. https://doi.org/10.1002/2013JD021040

Eck TF, Holben BN, Reid JS, Dubovik O, Smirnov A, O'Neill NT, Slutsker I, Kinne S (1999) Wavelength dependence of the optical

depth of biomass burning, urban, and desert dust aerosols. J Geophys Res 104:31333–31349

Eck TF, Holben BN, Dubovic O, Smirnov A, Goloub P, Chen HB, Chatenet B, Gomes L, Zhang XY, Tsay S-C, Ji Q, Giles D, Slutsker I (2005) Columnar aerosol optical properties at AERONET sites in central eastern Asia and aerosol transport to the tropical mid-Pacific. J Geophys Res 110:D06202. https://doi.org/10.1029/2004JD005274

Ferrare R, Ismail S, Browell E, Brackett V, Clayton M, Kooi S, Melfi SH, Whiteman D, Schwemmer G, Evans K, Russell P, Livingston J, Schmid B, Holben B, Remer L, Smirnov A, Hobbs PV (2000) Comparison of aerosol optical properties and water vapor among ground and airborne lidars and sun photometers during TARFOX. J Geophys Res 105(D8):9917–9933

Gautam R, Hsu NC, Kafatos M, Tsay SC (2007) Influences of Winter Haze on Fog/Low Cloud over the Indo-Gangetic Plains. J Geophys Res 112:D05207. https://doi.org/10.1029/2005JD007036

Gautam R, Hsu NC, Lau K-M, Tsay S-C, Kafatos M (2009) Enhanced pre-monsoon warming over the Himalayan-Gangetic region from 1979 to 2007. Geophys Res Lett 36:L07704. https://doi.org/10.1029/2009GL037641

Gautam R, Hsu NC, Lau KM (2010) Premonsoon aerosol characterization and radiative effects over the Indo-Gangetic Plains: implications for regional climate warming. J Geophys Res 115:D17208. https://doi.org/10.1029/2010JD013819.

Gautam R, Hsu NC, Tsay SC, Lau KM, Holben BN, Bell S, Smirnov A, Li C, Hansell R, Ji Q, Payra S, Aryal D, Kayastha R, Kim KM (2011) Accumulation of aerosols over the Indo-Gangetic Plains and southern slopes of the Himalayas: distribution, properties and radiative effects during the 2009 pre-monsoon season. Atmos Chem Phys 11:12841–12863

Gautam R, Hsu NC, Lau WK-M, Yasunari TJ (2013) Satellite observations of desert dust-induced Himalayan snow darkening. Geophys Res Lett 40:988–993

Giles DM, Holben BN, Tripathi SN, Eck T, Newcomb W, Slutsker I, Dickerson R, Thompson A, Mattoo S, Wang S, Singh RP, Sinyuk A, Schafer J (2011) Aerosol properties over the Indo-Gangetic plain: a 1 mesoscale perspective from the TIGERZ experiment. J Geophys Res 116:D18203. https://doi.org/10.1029/2011JD015809

Gobbi GP, Kaufman YJ, Koren I, Eck TF (2007) Classification of aerosol properties derived from AERONET direct sun data. Atmos Chem Phys 7:453–458

Gogikar P, Tyagi B (2016) Assessment of particulate matter variation during 2011 -2015 over a tropical station Agra, India. Atmos Environ 147:11–21

Gogoi MM, Moorthy KK, Babu SS, Bhuyan PK (2009) Climatology of columnar aerosol properties and the influence of synoptic conditions: First-time results from the northeastern region of India. J Geophys Res 114:D08202. https://doi.org/10.1029/2008JD010765

Gogoi M, Pathak B, Moorthy KK, Bhuyan PK, Suresh Babu S, Bhuyan K, Kalita G (2011) Mutli-year investigations of near surface and columnar aerosols over Dibrugarh, north-eastern location of India: heterogeneity in source impacts. Atmos Environ 45:1714–1724

Grandey BS, Siter P, Wagner TM (2013) Investigating relationship between aerosol optical depth and cloud fraction using satellite, aerosol reanalysis and general circulation model data. Atmos Chem Phys 13:3177–3184

Guleria RP, Kuniyal JC, Sharma NL, Dhyani PP (2012) Seasonal variability in aerosol optical and physical characteristics estimated using the application of the Angstrom formula over Mohal in the northwestern Himalaya, India. J Earth Syst Sci 121(3):697–710

Habib G, Venkataraman C, Bond TC, Schauer JJ (2008) Chemical, microphysical and optical properties of primary particles from the combustion of biomass fuels. Environ Sci Technol 42(23):8829–8834

Huang J, Lin B, Minnis P, Wang T, Wang X, Hu Y, Yi Y, Ayers JK (2006) Satellite-based assessment of possible dust aerosols semi-direct effect on cloud water path over East Asia. Geophys Res Lett 33: L19802. https://doi.org/10.1029/2006GL026561

IPCC: Fifth Assessment Report: Climate Change (2013) Cambridge University Press, New York, NY, USA, 2013.

Kang NA, Kumar KR, Hu K, Yu X, Yin Y (2016) Long-term (2002–2014) evolution and trend in collection 5.1 Level-2 aerosol products derived from the MODIS and MISR sensors over the Chinese Yangtze River Delta. Atmos Res 181:29–43

Kannemadugu HBS, Joshi AK, Moharil SV (2014) Aerosol optical properties and types over Nagpur, Central India. Sustain Environ Res 24(1):29–40

Kannemadugu HBS, Varghese AO, Mukkara SR, Joshi AK, Moharil SV (2015) Discrimination of aerosol types and validation of MODIS aerosol and water vapour products using a sun photometer over Central India. Aerosol Air Qual Res 15:682–693

Kaskaoutis DG, Kambezidis HD (2006) Investigation on the wavelength dependence of the aerosol optical depth in the Athens area. Q J R Meteorol Soc 132:2217–2234

Kaskaoutis DG, Kambezidis HD, Hatzianastassiou N, Kosmopoulos PG, Badarinath KVS (2007) Aerosol climatology: dependence of the Angstrom exponent on wavelength over four AERONET sites. Atmos Chem Phys Discuss 7:7347–7397

Kaskaoutis DG, Badarinath KVS, Kharol SK, Sharma AR, Kambezidis HD (2009) Variations in the aerosol optical properties and types over the tropical urban site of Hyderabad. J Geophys Res 114:D22204. https://doi.org/10.1029/2009JD012423

Kaskaoutis DG, Kalapureddy MCR, Krishna Moorthy K, Devara PCS, Nastos PT, Kosmopoulos PG, Kambezidis HD (2010) Heterogeneity in pre-monsoon aerosol types over the Arabian Sea deduced from ship-borne measurements of spectral AODs. Atmos Chem Phys 10:4893–4908

Kaskaoutis DG, Kharol SK, Sinha PR, Singh RP, Kambezidis HD, Sharma AR, Badarinath KVS (2011) Extremely large anthropogenic-aerosol contribution to total aerosol load over the Bay of Bengal during winter season. Atmos Chem Phys 11:7097–7117

Kaskaoutis DG, Gautam R, Singh RP, Houssos EE, Goto D, Singh S, Bartzokas A, Kosmopoulos PG, Sharma M, Hsu NC, Holben BN, Takemura T (2012a) Influence of anomalous dry conditions on aerosols over India: transport, distribution and properties. J Geophys Res 117:D09106. https://doi.org/10.1029/2011JD017314

Kaskaoutis DG, Singh RP, Gautam R, Sharma M, Kosmopoulos PG, Tripathi SN (2012b) Variability and trends of aerosol properties over Kanpur, Northern India using AERONET data (2001-10). Environ Res Lett 7:024003

Kaskaoutis DG, Sinha PR, Vinoj V, Kosmopoulos PG, Tripathi SN, Misra A, Sharma M, Singh RP (2013) Aerosol properties and radiative forcing over Kanpur during severe aerosol loading conditions. Atmos Environ 79:7–19

Kaskaoutis DG, Houssos EE, Goto D, Bartzokas A, Nastos PT, Sinha PR, Kharol SK, Kosmopoulos PG, Singh RP, Takemura T (2014a) Synoptic weather conditions and aerosol episodes over Indo-Gangetic Plains, India. Clim Dyn 43:2313–2331

Kaskaoutis DG, Kumar S, Sharma D, Singh RP, Kharol SK, Sharma M, Singh AK, Singh S, Singh A, Singh D (2014b) Effects of crop residue burning on aerosol properties, plume characteristics, and long-range transport over northern India. J Geophys Res Atmos 119:5424–5444

Kedia S, Ramchandran S (2011) Seasonal variations in aerosol characteristics over an urban location and a remote site in western India. Atmos Environ 45(12):2120–2128

Kharol SK, Badarinath KVS, Sharma AR, Mahalakshmi DV, Singh D, Krishna PV (2012) Black carbon aerosol variations over Patiala City, Punjab, India—a study during agriculture crop residue burning period using ground measurements and satellite data. J Atmos Sol Terr Phys 84–85:45–51

Komppula M, Mielonen T, Arola A, Korhonen K, Lihavainen H, Hyvärinen A-P, Baars H, Engelmann R, Althausen D, Ansmann A, Müller D, Panwar TS, Hooda RK, Sharma VP, Kerminen V-M, Lehtinen KEJ, Viisanen Y (2012) Technical note: one year of Raman-lidar measurements in GualPahari EUCAARI site close to New Delhi in India – seasonal characteristics of the aerosol vertical structure. Atmos Chem Phys 12:4513–4524

Kumar R, Naja M, Satheesh SK, Ojha N, Joshi H, Sarangi T, Pant P, Dumka UC, Hegde P, Venkataramani S (2011) Influences of the springtime northern Indian biomass burning over the central Himalayas. J Geophys Res 116:D19302. https://doi.org/10.1029/2010JD015509.

Kumar M, Tiwari S, Murari V, Singh AK, Banerjee T (2015) Wintertime characteristics of aerosols at middle Indo-Gangetic plain: impacts of regional meteorology and long range transport. Atmos Environ 104: 162–175

Lau KM, Kim MK, Kim KM (2006) Asian summer monsoon anomalies induced direct forcing: the role of the Tibetan plateau. Clim Dyn 26(7–8):855–864

Lawrence MG, Lelieveld J (2010) Atmospheric pollutant outflow from southern Asia: a review. Atmos Chem Phys 10(22):11017–11096

Lee J, Kim J, Song CH, Kim SB, Chun Y, Sohn BJ, Holben BN (2010) Characteristics of aerosol types from AERONET sun photometer measurements. Atmos Environ 44:3110–3117

Li C, Hu Y, Zhang F, Chen J, Ma Z, Ye X, Yang X, Wang L, Tang X, Zhang R, Mu M, Wang G, Kan H, Wang X, Mellouki A (2017) Multi-pollutant emissions from the burning of major agricultural residues in China and the related health-economic effects. Atmos Chem Phys 17:4957–4988

Lin J, Li J (2016) Spatio-temporal variability of aerosols over East China inferred by merged visibility-GEOS-Chem aerosol optical depth. Atmos Environ 132:111–122

Lodhi NK, Beegum SN, Singh S, Kumar K (2013) Aerosol climatology at Delhi in the western Indo-Gangetic Plain: microphysics, long-term trends, and source strengths. J Geophys Res 118:1361–1375. https://doi.org/10.1002/jgrd.50165

Mahowald N (2011) Aerosol indirect effect on biogeochemical cycles and climate. Science 334(6057):794–796

Ming L, Jin L, Li J, Fu P, Yang W, Liu D, Zhang G, Wang Z, Li X (2017) $PM_{2.5}$ in the Yangtze River Delta, China: chemical compositions, seasonal variations, and regional pollution events. Environ Pollut 223:200–212

Mishra AK, Shibata T (2012) Climatological aspects of seasonal variation of aerosol vertical distribution over central Indo-Gangetic belt (IGB) inferred by the space borne lidar CALIOP. Atmos Environ 46:365–375

Misra A, Tripathi SN, Kaul D, Welton E (2012) Study of MPLNET derived aerosol climatology over Kanpur, India, and validation of CALIPSO level 2 version 3 backscatter and extinction products. J Atmos Ocean Technol 29:1285–1294

Moorthy KK et al (1999) Aerosol climatology over India. 1- ISRO GBP MWR network and database, ISRO/GBP, SR-03-99

Moorthy KK, Babu SS, Manoj MR, Satheesh SK (2013) Buildup of aerosols over Indian region. Geophys Res Lett 40:1011–1014

Morys M, Mims FM III, Hagerup S, Anderson SE, Baker A, Kia J, Walkup T (2001) Design, calibration, and performance of MICROTOPS II handheld ozone monitor and sun photometer. J Geophys Res 106:14573–14582

Myhre G, Berglen TF, Johnsrud M, Hoyle CR, Berntsen TK, Christopher SA, Fahey DW, Isaksen ISA, Jones TA, Kahn RA, Loeb N, Quinn P, Remer L, Schwarz JP, Yttri KE (2009) Modelled radiative forcing of the direct aerosol effect with multi-observation evaluation. Atmos Chem Phys 9:1365–1392

Pai DS and Bhan SC (2012) National Climate Monsoon (2012). IMD Met Monograph: Synoptic Meteorology No13/2013

Pandithurai G, Dipu S, Dani KK, Tiwari S, Bisht DS, Devara PCS, Pinker RT (2008) Aerosol radiative forcing during dust events over New Delhi. India J Geophys Res 113:D13209. https://doi.org/10.1029/2008JD009804

Pani SK, Verma S (2014) Variability of winter and summertime aerosols over eastern India urban environment. Atmos Res 137:112–124

Patel PN, Dumka UC, Kaskaoutis DG, Babu KN, Mathur AK (2017) Optical and radiative properties of aerosols over Desalpar, a remote site in western India: source identification, modification processes and aerosol type discrimination. Sci Total Environ 575:612–627

Porter JN, Miller M, Pietras C, Motell C (2001) Ship-based sun photometer measurements using Microtops sun photometers. J Atmos Ocean Technol 18:765–774

Prasad AK, Singh RP, Kafatos M (2006) Influence of coal based thermal power plants on aerosol optical properties in the indo-Gangetic basin. Geophys Res Lett 33:L05805. https://doi.org/10.1029/2005GL023801

Prasad AK, Singh S, Chauhan SS, Srivastava MK, Singh RP, Singh R (2007) Aerosol radiative forcing over the Indo-Gangetic Plains during major dust storms. Atmos Environ 41:6289–6301

Rajput P, Sarin MM, Sharma D, Singh D (2014) Characteristics and emission budget of carbonaceous species from post-harvest agricultural-waste burning in source region of the Indo-Gangetic plain. Tellus Ser B Chem Phys Meteorol 66:21026. https://doi.org/10.3402/tellusb.v66.21026

Ram K, Sarin MM, Tripathi SN (2010) A 1 year record of carbonaceous aerosols from an urban site in the Indo-Gangetic plain: characterization, sources and temporal variability. J Geophys Res 115:D24313. https://doi.org/10.1029/2010JD014188

Ram K, Singh S, Sarin MM, Srivastava AK, Tripathi SN (2016) Variability in aerosol optical properties over an urban site, Kanpur, in the Indo-Gangetic Plain: a case study of haze and dust events. Atmos Res 174 –175:52–61

Raman RS, Ramachandran S (2011) Source apportionment of the ionic components in precipitation over an urban region in Western India. Environ Sci Pollut Res 18:212–225

Ramanathan V, Ramana MV (2005) Persistent, widespread, and strongly absorbing haze over the Himalayan foothills and the Indo-Ganges plains. Pure Appl Geophys 162:1609–1626

Ramchandran S (2007) Aerosol optical depth and fine mode fraction variations deduced from Moderate Resolution Imaging Spectroradiometer (MODIS) over four urban areas in India. J Geophys Res. https://doi.org/10.1029/2007JD008500

Rashki A, Kaskaoutis DG, Rautenbach CJW, Flamant C, AbdiVishkaee F (2014) Spatio-temporal variability of dust aerosols over the Sistan region in Iran based on satellite observations. Nat Hazards 71:563–585

Reddy OB k, Balakrishnaih G, Rama Gopal K, Siva Kumar Reddy N, ChakradharRao T, Lokeswara Reddy T, NazeerHussain S, Vasudeva Reddy M, Reddy RR, Boreddy SKR, Suresh Babu S (2016) Long term (2007 - 2013) observations of columnar aerosol optical properties and retrieved size distributions over Anantapur, India using multi wavelength solar radiometer. Atmos Environ 142:238–0250

Rehman IH, Ahmed T, Praveen PS, Kar A, Ramanathan V (2011) Black carbon emissions from biomass and fossil fuels in rural India. Atmos Chem Phys 11:7289–7299

Reid JS, Eck TF, Christopher SA, Hobbs PV, Holben BN (1999) Use of the Angstrom exponent to estimate the variability of optical and physical properties of aging smoke particles in Brazil. J Geophys Res 104(D22):473–489

Rosenfeld D, Lohmann U, Raga GB, O'Dowd CD, Kulmala M, Fuzzi S, Reissell A, Andreae MO (2008) Flood or drought: how do aerosols affect precipitation? Science 321(5894):1309–1313

Russell PB, Bergstrom RW, Shinozuka Y, Clarke AD, De-Carlo PF, Jimenez JL, Livingston JM, Redemann J, Dubovik O, Strawa A (2010) Absorption Angstrom Exponent in AERONET and related

data as an indicator of aerosol composition. Atmos Chem Phys 10: 1155–1169

Sarkar S, Chokngamwong R, Cervone G, Singh RP, Kafatos M (2006) Variability of aerosol optical depth and aerosol forcing over India. Adv Space Res 37(12):2153–2159

Satheesh SK, Ramanathan V, Holben BN, Moorthy KK, Loeb NG, Maring H, Prospero GM, Savoie D (2002) Chemical, microphysical, and radiative effects of Indian Ocean aerosols. J Geophys Res 107(D23):4725. https://doi.org/10.1029/2002JD002463

Satheesh SK, Moorthy KK, Kaufman YJ, Takemura T (2006) Aerosol optical depth, physical properties and radiative forcing over the Arabian Sea. Meteorog Atmos Phys 91:45–62

Schuster GL, Dubovik O, Holben BN (2006) Angstrom exponent and bimodal aerosol size distributions. J Geophys Res 111:D07207. https://doi.org/10.1029/2005JD006328

Schwartz SE, Arnold F, Blanchet J-P, Durkee PA, Hofmann DJ, Hoppel WA, King MD, Laos AA, Nakajima T, Ogren JA, Toon OB, Wendisch M (1995) Group report: connections between aerosol properties and forcing of climate. John Wiley, Hoboken, pp 251–280

Seinfeld JH et al (2016) Improving our fundamental understanding of the role of aerosol−cloud interactions in the climate system. PNAS 113(21):5781–5790

Sharma AR, Kharol SK, Badarinath KVS, Singh D (2010) Impact of agriculture crop residue burning on atmospheric aerosol loading—a study over Punjab State, India. Ann Geophys 28:367–379

Sharma D, Singh D, Kaskaoutis DG (2012) Impact of two intense dust storms on aerosol characteristics and radiative forcing over Patiala, northwestern India. Adv Meteorol. https://doi.org/10.1155/2012/956814

Sharma M, Kaskaoutis DG, Singh RP, Singh S (2014) Seasonal variability of atmospheric aerosol parameters over Greater Noida using ground sunphotometer observations. Aerosol Air Qual Res 14: 608–622

Singh S, Beegum SN (2013) Direct radiative effects of an unseasonal dust storm at a western Indo Gangetic Plain station Delhi in ultraviolet, shortwave, and longwave regions. Geophys Res Lett 40:2444–2449

Singh RP, Dey S, Tripathi SN, Tare V, Holben BN (2004) Variability of aerosol parameters over Kanpur, northern India. J Geophys Res 109: D23206. https://doi.org/10.1029/2004JD004966

Singh S, Soni K, Bano T, Tanwar RS, Nath S, Arya BC (2010) Clear-sky direct aerosol radiative forcing variations over mega-city Delhi. Ann Geophys 28:1157–1166

Singh A, Tiwari S, Sharma D, Singh D, Tiwari S, Srivastava AK, Rastogi N, Singh AK (2016) Characterization and radiative impact of dust aerosols over north-western part of India: a case study during a severe dust storm. Meteorog Atmos Phys 128(6):779–792

Sinha PR, Kaskaoutis DG, Manchanda RK, Sreenivasan S (2012) Characteristics of aerosols over Hyderabad, in Southern Peninsular India with the use of different techniques. Ann Geophys 30:1393–1410

Sinha PR, Manchanda RK, Kaskaoutis DG, Kumar YB, Sreenivasan S (2013) Seasonal variation of surface and vertical profile of aerosol properties over a tropical urban station Hyderabad, India. J Geophys Res 118:749–768

Moorthy KK, Babu SS, Satheesh SK (2007) Temporal heterogeneity in aerosol characteristics and the resulting radiative impact at a tropical coastal station—Part 1: Microphysical and optical properties. Ann Geophys 25(11):2293–2308

Soni K, Singh S, Tanwar RS, Nath S (2011) Wavelength dependence of the aerosol angstrom exponent and its implications over Delhi, India. Aerosol Sci Technol 45:1488–1498

Srivastava R, Ramachandran S (2013) The mixing state of aerosols over the Indo-Gangetic Plain and its impact on radiative forcing. Q J R Meteorol Soc 139:137–151

Srivastava AK, Tiwari S, Devara PCS, Bisht DS, Srivastava MK, Tripathi SN, Goloub P, Holben BN (2011) Pre-monsoon aerosol characteristics over the Indo-Gangetic basin: implications to climatic impact. Ann Geophys 29:789–804

Tiwari S, Singh AK (2013) Variability of aerosol parameters derived fromground and satellite measurements over Varanasi located in Indo–Gangetic basin. Aerosol Air Qual Res 13:627–638

Tiwari S, Srivastava AK, Bisht DS, Bano T, Singh S, Behura S, Srivastava MK, Chate DM, Padmanabhamurty B (2009) Black carbon and chemical characteristics of PM10 and PM2.5 at an urban site of North India. J Atmos Chem 62(3):193–209

Tiwari S, Srivastava AK, Singh AK (2013) Heterogeneity in pre-monsoon aerosol characteristics over the Indo-Gangetic Basin. Atmos Environ 77:738–747

Tiwari S, Srivastava AK, Singh AK, Singh S (2015a) Identification of aerosol types over Indo-Gangetic Basin: implications to optical properties and associated radiative forcing. Environ Sci Pollut Res 22(16):12246–12260

Tiwari S, Hopke PK, Pipal AS, Srivastava AK, Bisht DS, Shani T, Singh AK, Soni VK, Attri SD (2015b) Intra-urban variability of particulate matter ($PM_{2.5}$and PM_{10}) and its relationship with optical properties of aerosols over Delhi, India. Atmos Res 166:223–232

Tiwari S, Tiwari S, Hopke PK, Attri SD, Soni VK, Singh AK (2016a) Variability in optical properties of atmospheric aerosols and their frequency distribution over a mega city "New Delhi", India. Environ Sci Pollut Res 23:8781–8793

Tiwari S, Mishra AK, Singh AK (2016b) Aerosol climatology over the Bay of Bengal and Arabian Sea inferred from Space-borne Radiometers and Lidar Observations. Aerosol Air Qual Res 16: 2855–2868

Twomey S (1991) Aerosols, clouds, and radiation. Atmos Environ 25: 2435–2442

Vadrevu KP, Ellicott E, Giglio L, Badarinath KVS, Vermote E, Justice C, Lau WKM (2012) Vegetation fires in the Himalayan region—aerosol load, black carbon emissions and smoke plume heights. Atmos Environ 47:241–251

Vaughan JM, Maryon RH, Geddes NJ (2002) Comparison of atmospheric aerosol backscattering and air mass back trajectories. Meteorog Atmos Phys 79:33–46

Vaishya A, Singh P, Rastogi S, Babu SS (2017) Aerosol black carbon quantification in the central Indo-Gangetic Plain: seasonal heterogeneity and source apportionment. Atmos Res 185:13–21

Xin Y, Wang G, Chen L (2016) Identification of long-range transport pathways and potential apportionment of fine organic aerosols in Beijing s of PM_{10} in Tibetan Plateau uplift area: case study of Xining, China in 2014. Aerosol Air Qual Res 16(4):1044–1054

Yao L, Yang L, Yuana Q, Yana C, Dong C, Meng C, Sui X, Yang F, Lu Y, Wang W (2016) Sources apportionment of $PM_{2.5}$ in a background site in the North China Plain. Sci Total Environ 541:590–598

Zheng Y, Che H, Zhao T, Zhao H, Gui K, Sun T, An LY, Chong L, Jiang Y, Zhang L, Wang H, Wang Y, Zhang X (2017) Aerosol optical properties observation and its relationship to meteorological conditions and emission during the Chinese National Day and Spring Festival holiday in Beijing. Atmos Res 197:188–200